Examining Paleoclimate Interpretations of Saharan Aeolian Dust Fluxes Using Modern Observations

A Thesis Presented

by

Candice F. Z. Chen

to

the Department of Earth and Planetary Sciences

in partial fulfillment of the requirements

for a degree with honors of Bachelor of Arts

April 2022

Harvard College

Abstract

Much of what we understand of past African climate comes from inferring aridity from aeolian dust deposition in marine sediment cores. The interpretation is simple: greater dust indicates periods of greater aridity. This view is challenged, however, by modern observations that dust export and deposition seem to be modulated by winds more than changes in vegetation. In this thesis, we leverage modern measurements of dust deposition, atmospheric dust concentration, vegetation cover, and winds to gauge what dust deposited offshore may actually indicate about regional circulation and vegetation. We conduct our analysis in three major parts. First, we inter-compare four dust deposition records to assess seasonality of deposition and reproducibility among records. Second, we evaluate the relationship between dust deposition and ambient atmospheric dust and wind conditions. Third, we assess the linkages between atmospheric dust and regional vegetation and surface winds. We find no clear deposition seasonal cycle, only moderate correspondence between atmospheric dust concentration and deposition, and seasonally variable influences of wind and vegetation on dust. Overall, winds are the dominant control on dust export during seasons of significant dust deposition. Therefore, aeolian dust flux seems to be more a proxy of tropical circulation than of aridity for our observation period. Our analysis of interannual variations cannot refute interpretations of centennial or millennial variations in marine sediment records, but this work sheds light on the lack of support modern observations lend to the traditional paleoclimatic interpretation of dust flux and underscores the need for more work to resolve the proper interpretation of the aeolian dust flux proxy.

Contents

List of Figures

Acknowledgements

First, I would like to thank Peter Huybers for advising this thesis. His steady guidance made this work possible, and I feel lucky to have a mentor with such lucid perspectives on science and on life.

Next, I must thank my mother, a brilliant scientist herself who is ever my inspiration and role model. She generously reviewed this manuscript.

Thank you to the EPS department for sustained support through the years, and in particular to Esther James and Chloe Anderson for scaffolding my thesis-writing process.

Finally, I extend my deepest thanks to my friends, whose radiant presence has made senior year—and really all of college—a joy.

Thank you all.

Chapter 1

Introduction

Today, we know the Sahara as the largest hot desert in the world—a tremendous sea of sand and salt flats. But merely 6,000 years ago, nearly all of North Africa was covered in rolling grasslands, dotted with deep lakes and acacia (Figure 1.1) (*Jolly et al.*, 1998; *Watrin et al.*, 2009). The savanna boasted abundant fauna and neolithic human communities which cultivated domesticated plants and animals (*Kuper and Kropelin*, 2006).

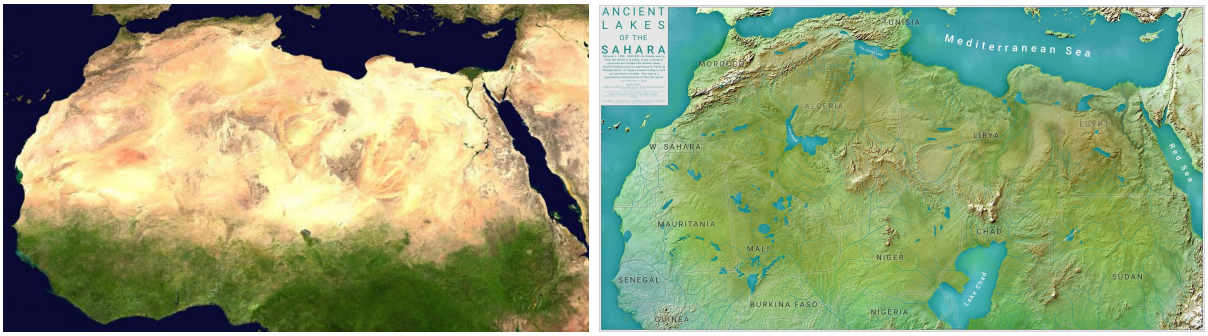

Figure 1.1: Left: Satellite image of North Africa (Source: *NASA*). Right: Speculative illustration of the Green Sahara (Source: *Carl Churchill*).

This was the most recent "African Humid Period," an interval defined by higher-than-modern rainfall across much of North Africa. For the past eight million years, North African hydroclimate has rapidly tipped in and out of African Humid Periods over 230 times, driven primarily by changes in Northern Hemisphere summer insolation modulated by Earth's orbital precession (*Larrasoaña et al.*, 2013; *deMenocal et al.*, 2000).

Humans evolved amidst—and perhaps because of—these rapid climate fluctuations. Environmental shifts have been invoked to explain morphological adaptation to bipedalism (*Senut et al.*, 2018), enlarged cranial capacity and emergence of stone tools (*Stanley*, 1992),

and behavioral adaptability which engendered cultural innovation (*Calvin*, 2003).

The variability selection hypothesis, a mode of natural selection, links the emergence of key human traits to adaptation triggered by dramatic climate variability. Rapid environmental fluctuations affect the survival and success of an organism and its offspring through time—only those that can weather a wide array of conditions will ultimately survive uncertain climate futures. Variability selection argues that the largest faunal speciation events should occur during intervals of highest environmental variability (*Potts*, 1998).

Indeed, there are indications that hominid speciation coincided with periods of high-amplitude paleoclimatic variability 2.9–2.4, 1.8–1.6, and 1.2–0.8 million years ago (*deMenocal*, 2004). These three periods approximately correspond with the emergence of *Australopithecus afarensis*, a primitive ape; *Homo habilis*, the first human species; and *Homo erectus*, the direct precursor to *Homo sapiens* which became skilled at using stone tools and hunting (*Wood*, 1996). Figure 1.2 illustrates the timeline of hominid evolution alongside African climate fluctuations. Beyond evolution, hominid migration within and eventually out of Africa was also paced by alternating humid and arid periods (*Drake et al.*, 2011; *Blome et al.*, 2012; *Tierney et al.*, 2017; *Schaebitz et al.*, 2021).

The most recent African Humid Period period lasted from about 14.8 until 5.5 thousand years before present (*deMenocal et al.*, 2000). Towards the end of this humid period, the progressive drying of the region drove populations out of North Africa and precipitated major societal shifts, including the fall of the Egyptian Old Kingdom and Akkadian Empire (*Brooks*, 2006; *Cullen et al.*, 2000). This termination is also thought to have spurred the beginning of pharaonic civilization along the Nile, a notable rise of complex social systems supported by sedentary agriculture (*Kuper and Kropelin*, 2006).

Ancient African climate had a pronounced influence on the origin of our species, human movement, and the rise and fall of civilizations. Paleoclimatic variations wove the very fabric of our species. In many ways, the back-and-forth between aridity and humidity is the pulse of early human history.

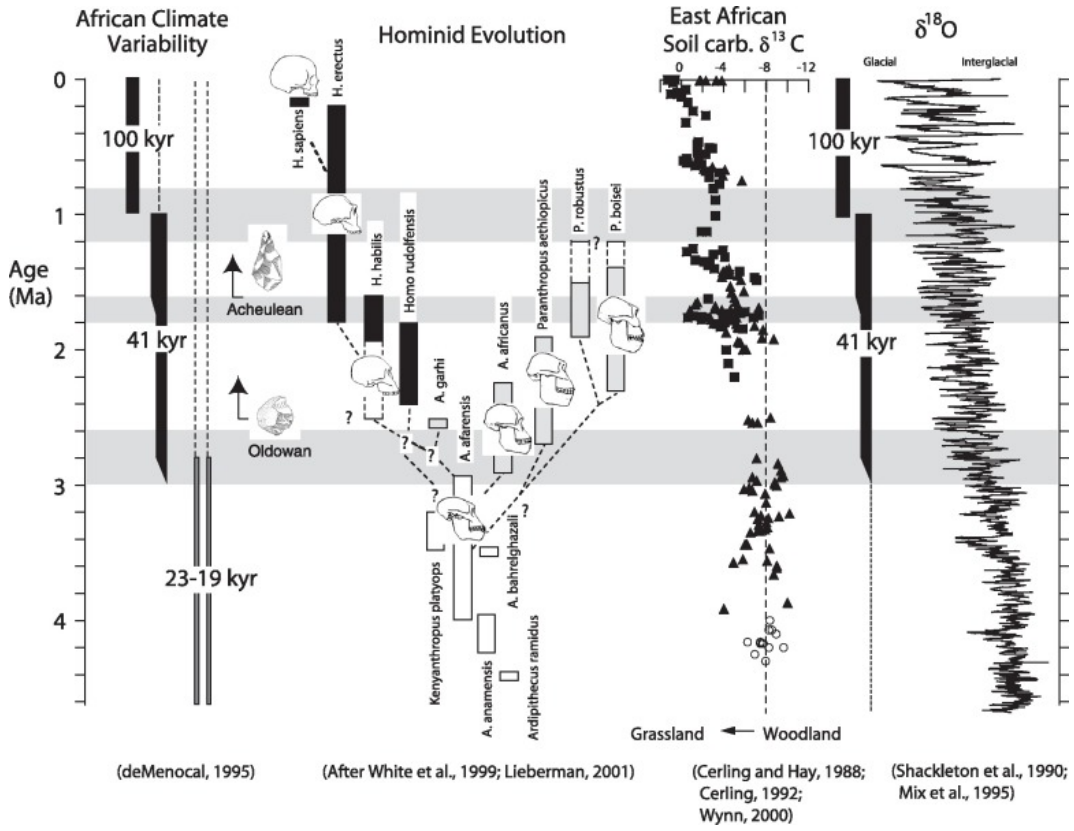

Figure 1.2: African paleoclimatic variations and hominid evolution events. High climatic variability intervals are shaded in gray. From *deMenocal* (2004).

Many have drawn inferences about the African Humid Period from the abundance of wind-blown dust present in marine sediment cores off the Northwest African coast (e.g., *deMenocal et al.*, 2000; *Ehrmann et al.*, 2017; *Zielhofer et al.*, 2017). Several other proxies have been used to reconstruct past aridity in North Africa, like geologic evidence of past lake basins (e.g., *Forman et al.*, 2014), oxygen isotope records of river outflow and precipitation (e.g., *Weldeab et al.*, 2005; *Gasse*, 2002), pollen records of paleovegetation (e.g., *Kropelin et al.*, 2008), hydrogen isotope records in leaf wax (e.g., *Tierney and deMenocal*, 2013), and speleothem records (e.g., *Hoffmann et al.*, 2016). However, these proxies do not offer the great temporal depth and continuity that dust deposition in marine sediments can deliver—temporal reach and resolution that are necessary to discern early human responses to climate at a sufficiently fine scale.

Aeolian, or wind-blown, dust is the key proxy for defining the African Humid Period. The seminal study defining the abrupt onset and termination of the African Humid Period, *deMenocal et al.* (2000), relies on the aeolian dust flux proxy applied to a marine sediment core off the coast of Mauritania (Figure 1.3). The African Humid Period is identified in this down-core record by an interval of low dust flux. *deMenocal et al.* (2000) made bold claims about past aridity based on dust fluxes through time, and this reasoning remains the hallmark of paleo-dust interpretations in the literature.

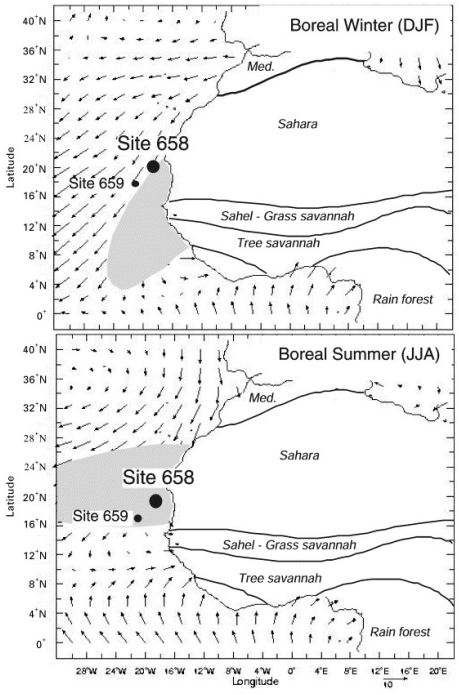

Figure 1.3: *deMenocal et al.* (2000) identified the sudden onset and termination of the African Humid Period with a sediment core record from Ocean Drilling Program Site 658C. Seasonal climatology of wind (arrows) and dust plume (shading) are shown for Northern Hemisphere winter (top) and summer (bottom). From *deMenocal et al.* (2000).

Paleoclimate studies that consider dust flux almost universally interpret that greater dust indicates increased aridity, while lower dust indicates increased humidity. However, studies based on modern variations point to other factors as being primary, raising the question of whether this proxy is being correctly interpreted. Aeolian dust flux has a variety of influences besides vegetation cover, including properties of the source region and wind patterns. In particular, winds are thought to be the dominant control on dust emission and export. *Parker et al.* (2016) posit that wind strength, not changes in monsoon moisture delivery, primarily drove Saharan dust emissions over the last deglaciation (∼20,000 years). Using modern measurements, *Ridley et al.* (2014) claim that atmospheric dust flux is almost entirely mediated by surface wind, while land use and vegetation cover are not directly linked to dust export. The extent to which continental greenness enters the

marine dust deposition picture is an open question.

Furthermore, there is not a straightforward link between atmospheric dust concentration and dust deposition. Dust deposition depends very strongly on vertical dust distribution and wind speed (*Schepanski et al.*, 2009; *Figgis et al.*, 2018). In addition to having dust present in the atmosphere, the right conditions must be present for it to be deposited. This means that Northwest Africa can experience extremely dusty conditions without a corresponding increase in dust deposition off the coast. Favorable conditions for dust lofting—high winds—are also favorable conditions for long-distance transport and low deposition near the continental margin.

Dust deposition as a proxy for regional aridity is critical to the study of past African hydroclimate, yet reducing the complexity of dust to a simple indicator of aridity runs counter to observations of the modern system. The correspondence between land vegetation and offshore dust deposition have not yet been explored with modern measurements. In this thesis, we assess the extent to which dust deposition actually corresponds to regional aridity.

There are three steps that constitute dust's journey from the continental surface to the sea: dust must be lofted into the atmosphere, transported, then deposited into the ocean. Each of these steps have complex dynamical controls, introducing noise to the aridity-dust signal. We will consider each step to investigate the support modern observations lend to the assumed correspondence of continental aridity to dust deposition. In Chapter 2, we evaluate contemporary marine records of dust deposition. In Chapter 3, we discuss linkages between these dust flux records and atmospheric dust concentrations. In Chapter 4, we assess the relationship between atmospheric dust concentrations and land surface characteristics. We conclude in Chapter 5 where we assess our array of evidence in context of the complete paleoclimatic picture of aeolian dust flux as a proxy for aridity.

Chapter 2

Marine Records of Dust Deposition

We begin with the modern analogue of dust deposition records in marine sediment cores: dust deposition recorded in sediment traps. Part of the novelty of this work rests on gathering and comparing disparate modern deposition records that are not typically assessed relative to one another. Deposition records do not have the continuous spatial coverage of satellite-observed or modeled dust deposition, but we use in situ dust flux because most satellite estimates differ from recorded deposition by a factor of two, and model estimates differ from satellite estimates by factors of two to five (*Yu et al.*, 2019).

However, drawing from deposition records brings certain challenges. First, dust deposition records are sparse; our analysis would be greatly enriched if we had data from more locations. The other natural limitation of these records is their narrow temporal scale—they each last from one to three years. African dust export and winds have high seasonal variability, so we would ideally have several years of data per site to gauge the seasonal and interannual variations adequately.

Additionally, the sites are hard to compare against each other due to their different locations and different methods the authors used to isolate the land-sourced dust component of the sediment samples. There were two methods used to measure dust flux: residual-mass flux and dust-mass flux. In the dust-mass flux method, all biogenic components are chemically removed from the sediment sample so that only dust remains to be directly weighed (*van der Does et al.*, 2020). Since this is a direct measurement of dust mass, it is the truer representation of actual dust flux. Residual-mass flux is an estimate of the mineral dust fraction in sediment samples that is calculated by subtracting weights of biogenic constituents

from the total sample mass:

$$\text{residual mass} = \text{total mass} - \text{carbonate} - \text{opal} - 2 \times \text{C}_{\text{org}}$$

where $2 \times \text{C}_{\text{org}}$ is an estimate for organic matter mass because about 50-60% of marine organic matter is made of organic carbon (*Hedges et al.*, 2002). The carbonate, opal, and organic matter mass fractions are determined using calculation factors that are not globally well-constrained, so residual–mass flux is an indirect way of obtaining the mineral dust fraction that bears several uncertainties related to these conversion factors and measurements of biogenic components. The residual fraction usually overestimates the mineral dust fraction, as it can also include biogenic phosphates and sulfates, volcanic particles, and crystal water associated with opaline silica and clay minerals (*Korte et al.*, 2017).

Half of the marine sites we draw from (CB-24, CBi-11, CBi-12, and CV3) report residual-mass flux, while the other half (M1, M2, M3, and M4) report dust-mass flux. Despite their differences, the two methods each should preserve relative change in dust deposition through time. Three sites (M1, M2, and M4) have data published for the same interval in 2013 from both residual-mass fraction processing (*Korte et al.*, 2017) and dust-mass fraction processing (*van der Does et al.*, 2020). *van der Does et al.* (2020) reported that while the dust-mass fluxes are much smaller than residual-mass fluxes, they have good correlation (R^2 values of 0.73, 0.69, and 0.78), with slopes decreasing the farther a site is from the coast (Figures 2.1 and 2.2). For all three sites, the residual-mass flux is larger than the dust-mass

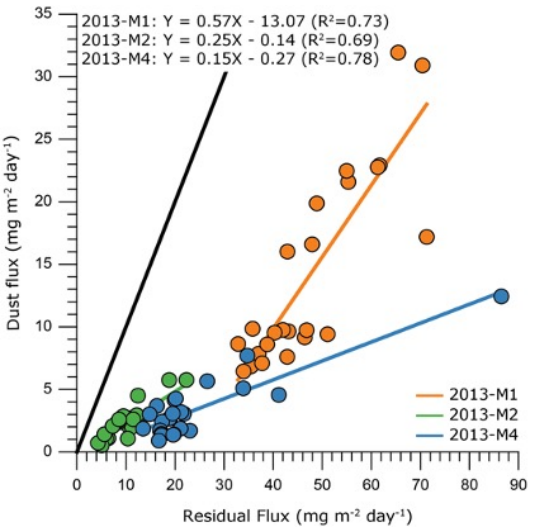

Figure 2.1: Dust-mass flux (*van der Does et al.*, 2020) versus residual-mass flux (*Korte et al.*, 2017) for sites M1, M2, and M4. The black line represents a 1:1 relation.

flux.

Only two of the four datasets, which include eight deposition sites, have overlap in their sampling periods. We discuss their correspondence in that overlap window later in this chapter. We also include a land-based deposition record in Mbour, Senegal, because it is close to the marine sites and has a longer record lasting three years.

Because of the restrictions imposed by low sampling period overlap, inconsistent dust isolation methods, and different locations, we cannot combine and calibrate these observations to create a longer time series of deposition. Instead, we consider each site independently in later analysis. Despite their limitations, they can collectively deliver critical insight to better understanding the nature of dust deposition off Northwest Africa.

The following sections report the details of each dust deposition dataset. Figure 2.2 is a map of the sites. Table 2.1 contains summary information for all sites.

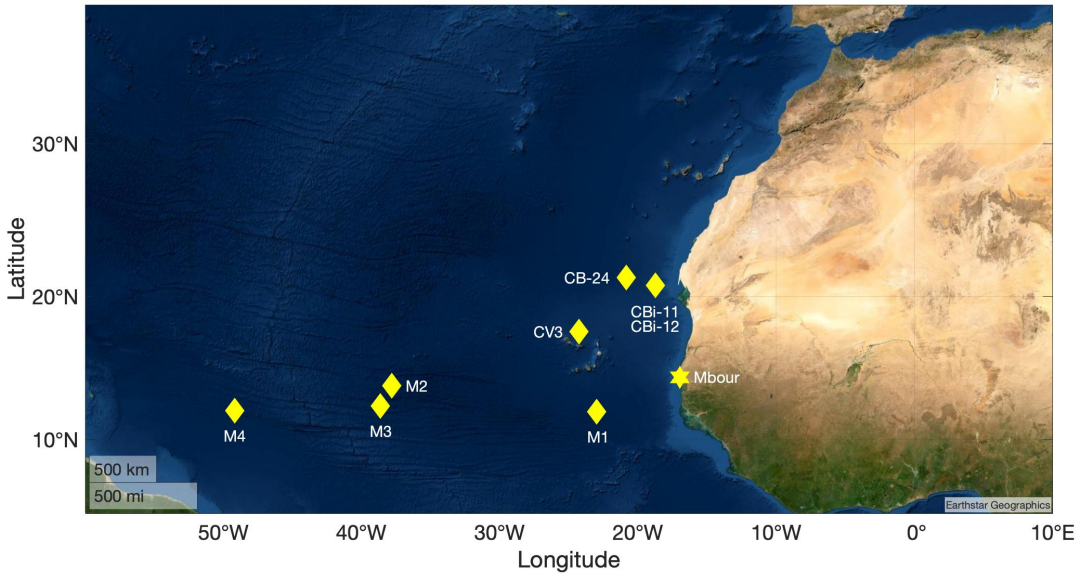

Figure 2.2: Locations of all deposition sites. Marine sites are marked with diamonds, while the coastal land site is marked with a star.

Trap	Location	Observation Period	Source
M1	12° N, 23° W	10/19/2012 - 3/31/2014	*van der Does et al.* (2020)
M2	13°49' N, 37°49' W	10/19/2012 - 10/25/2014	*van der Does et al.* (2020)
M3	12°24' N, 38°38' W	12/1/2013 - 10/17/2014	*van der Does et al.* (2020)
M4	12°2' N, 49°13' W	10/19/2012 - 10/25/2014	*van der Does et al.* (2020)
CB-24	21°17' N, 20°51' W	1/24/2013 - 2/5/2014	*Friese et al.* (2017)
CBi-11	20°46' N, 18°44' W	1/29/2013 - 3/25/2014	*Friese et al.* (2017)
CBi-12	20°46' N, 18°45' W	2/14/2014 - 2/23/2015	*Friese et al.* (2017)
CV3	17°59' N, 24°15' W	12/1/2009 - 10/4/2012	*Romero et al.* (2016)
Mbour	14°24' N, 16°57' W	2/23/2006 - 3/19/2009	*Skonieczny et al.* (2013)

Table 2.1: Summary information for dust deposition records.

2.1 Sediment Trap Site Descriptions

2.1.1 Sites M1, M2, M3, and M4

This record was published in *van der Does et al.* (2020) and was originally used to investigate dominant deposition pathways for dust in the Saharan plume. Sites M1, M2, M3, and M4 lie approximately along a transect at 12° N, with respective longitudes of 23° W, 37°49' W, 38°38' W, and 49°13' W. All sediment traps were moored at ∼1,200 m depth. M1 sampled from October 2012 - March 2014, M2 and M4 sampled from October 2012 - October 2014, and M3 sampled from December 2013 - October 2014. Sampling intervals ranged from 8 - 16 days. Dust was isolated from the samples by the dust-mass flux method.

2.1.2 Sites CB-24, CBi-11, and CBi-12

Friese et al. (2017) published this record, using it to refine dust provenance regions from geochemical signatures. Marine sediment traps at sites CBi-11 and CBi-12 were moored at approximately 20°46' N, 18°45' W with respective depths of 2800 m and 2750 m. CB-24 was located at 21°17' N, 20°51' W, 4160 m deep. Sampling spanned January 2013 - February 2014 for CB-24, January 2013 - March 2014 for CBi-11, and February 2014 - February 2015

for CBi-12. Sampling intervals ranged from 12 to 21 days. Dust flux was estimated using the residual-mass flux method.

2.1.3 Site CV3

This record was published by *Romero et al.* (2016) and was assessed in relation to diatom productivity. Site CV3 (17°59' N, 24°15' W) was moored at 1300 m depth and sampled from December 2009 - October 2012. Sampling intervals ranged from 27 to 29 days, and dust flux was estimated with the residual-mass flux method.

2.1.4 Mbour Site

Skonieczny et al. (2013) published this record to investigate deposition seasonality and geochemical provenance signatures. This is the only land-based dust collection site. Mineral dust was collected 8 m above ground atop a roof (14°24' N, 16°57' W). The site was located in a protected ecological center with low car traffic, minimizing the influence of locally-produced dust. Sampling took place from February 2006 through March 2009 with intervals ranging from two to eight days. Since dust collected at marine sites at similar latitudes is mainly >30 μm, samples were wet-sieved to remove particles larger than 30 μm which are most likely of local origin (i.e. vegetation detritus).

2.2 Deposition Time Series

The dust deposition records have highly variable sampling frequencies, ranging from a couple days to nearly a month. Our analysis in Chapters 3 and 4 draw from data at monthly time resolution, so we bin these deposition records to the monthly level in order to have all data on the same timescale. We calculated monthly average dust deposition for each site by averaging observations within each month, weighing by the duration of each observation within the month. Here, we present the binned time series for all sites (Figure 2.3).

Figure 2.3: Time series of monthly-averaged deposition for all sites, separated by publication source: (a) *van der Does et al.* (2020) spans October 2012 - October 2014, (b) *Friese et al.* (2017) spans February 2013 - February 2015, (c) *Romero et al.* (2016) spans December 2009 - September 2012, and (d) *Skonieczny et al.* (2013) spans February 2006 - March 2009. The x-axis is marked according to the central month in each season (i.e. January for winter, April for spring, etc.). Deposition for sites in (a) primarily peaked in summer, and there is a pronounced deposition flux drop-off for sites west of M1. Sites in (b) have mixed seasonalities, with peaks in summer, winter, and early spring. Site CV3 (c) had winter and early spring peaks. The Mbour site (d) had peak deposition around summer and spring.

Sites M1, M2, M3, and M4 all recorded highest flux during summer and early autumn,

coincident with seasonality of highest dust export from the continent (*Prospero and Carlson*, 1972). The seasonal amplitudes of traps M2, M3, and M4 are much lower than M1, consistent with the expectation that dust deposition decreases precipitously with distance from the source. Site CBi-11 recorded highest flux in late spring and summer, CBi-12 recorded peaks in late winter and early spring, and CB-24 recorded highest flux during early spring and early fall. Interestingly, site CV3 only had peaks during late winter and early spring, when dust export from the continent is usually at its lowest (*Prospero and Carlson*, 1972). The land-based collector at Mbour recorded highest deposition during early spring and summer, but there was high variation in seasonal deposition across the three-year record.

High deposition fluxes in winter and spring among many sites are likely due to dust transport occurring at lower latitudes during these seasons. In winter and spring, low level trade winds, called the harmattan, transport dust. In summer, dust is carried in the Saharan Air Layer which sits above the trade winds at ∼6 km altitude (*Skonieczny et al.*, 2013). Winter and spring deposition from lower-altitude dust may also be constituted of more dust from regions closer to the site of deposition (*van der Does et al.*, 2016).

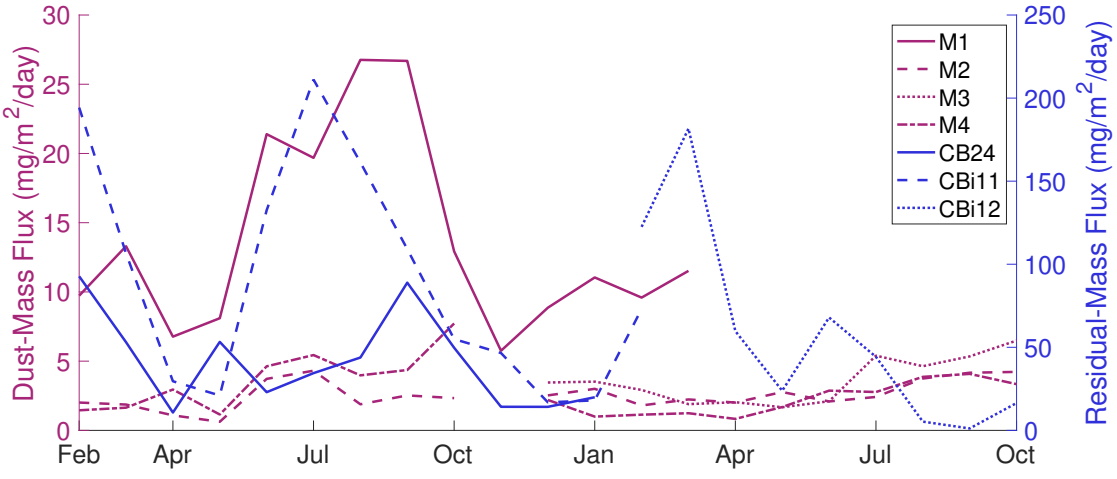

Figure 2.4: Overlap interval of deposition records from *van der Does et al.* (2020) and *Friese et al.* (2017) during February 2013 - October 2014. Sites M1, CBi-11, and CB-24 all record relatively high deposition flux in the summer.

Intervals of the time series from sites M1, M2, M3, M4, CB-24, CBi-11, and CBi-12

overlap in the window February 2013 - October 2014. These time series are plotted together in Figure 2.4 with different y-axes due to different methods of isolating the dust fraction of the sediment. Sites M1, CB-24, CBi-11, and CBi-12 are geographically closest, but we also include sites M2, M3, and M4 for completeness. CBi-11 and CB-24 respectively record peaks in July and September. M1 records high fluxes from June - September, which approximately coincide with the CBi-11 and CB-24 peaks. There is also relatively lower dust flux recorded by all three sites in April, November, and December of 2013. These correspondences lend support to the idea that the relative magnitudes of different deposition fluxes are preserved independent of method for isolating the dust component.

2.3 Discussion

This is the first inter-comparison of dust deposition records to assess seasonal correspondence and reproducibility. Many studies compile collections of dust deposition records in order to evaluate performance of satellite and model-estimated dust deposition flux (e.g., *Yu et al.*, 2019). However, they do not compare deposition time series and coherence among the records themselves. They instead compare annual and seasonal averages of individual records to satellite and model estimates.

We find that seasonal deposition cycles are quite incoherent among the nine sites, with peaks in winter and spring nearly as common as peaks during summer, when there is maximum dust export from the continent. This suggests that atmospheric dust concentration is not itself the dominant control on dust deposition. Additionally, the sites that were sampled over the same 2013 interval underscore location-dependent dust deposition variations. These inconsistencies would likely be smoothed in a longer record, but we must note that the data we have is highly variable.

We also do not address dust's journey from sea surface to seafloor, where the sediments are ultimately committed to sediment record. Currents and sediment perturbation each influence

dust's final resting place within ocean sediment, but we cannot address these processes within the scope of this thesis. It would also be interesting to better understand the effect of different sampling depths. Our marine sites range from 1200 - 4160 m deep, but we do not have enough consistency among sites to draw meaningful conclusions about the possible effects of sampling at different depths.

Our analysis is very limited by the short observation periods for each site. Ideally, we would have more years of data so that we could better evaluate the nature of the deposition seasonal cycle year over year. Using model or satellite estimates of deposition would significantly improve spatial and temporal coverage, but it would come at the great expense of accuracy as estimated deposition flux is highly uncertain. These observations, despite their limitations, serve as the foundation for our analysis in the next chapter, grounding satellite-measured dust concentrations in recorded deposition.

Chapter 3

Linkages Between Marine Dust Deposition and Atmospheric Dust Concentrations

In this chapter, we assess the relationship between dust deposition and ambient dust and wind conditions. We begin with a brief discussion of the seasonal prevailing wind and dust patterns to build a contextual foundation from which we can best interpret our results.

Three major atmospheric circulation patterns over North Africa modulate the outflow of Saharan and Sahelian dust to the Atlantic: the harmattan, the Saharan heat low, and the West African monsoon (*Schepanski et al.*, 2017). Each has a distinct seasonal pattern. The harmattan is the northeasterly trade wind system over North Africa and is driven by the continental pressure gradient between the Intertropical Convergence Zone and the subtropical subsidence zone. The harmattan dominates circulation from November through February (*Pinker et al.*, 1994). The Saharan heat low is a thermal low formed from intense heating over the desert surface and peaks in mid-summer (*Chauvin et al.*, 2010). The West African monsoon is a monsoonal circulation driven by land-sea temperature contrasts. It transports cool, moist air from the Gulf of Guinea into North Africa in the summer. In the winter, it reverses to dry northeasterly harmattan winds. Seasonal climatologies of 10-m and 850-hPa winds are included in the Appendix (Figures A.2 and A.3) for reference.

Westward dust export from North Africa over the northern equatorial Atlantic (Figure 3.1) happens throughout the year and peaks in the late spring, summer, and early fall (*Prospero and Carlson*, 1972). High dust export in the summer results from strong surface turbulence associated with monsoonal frontal systems. Dust is convectively lifted and trans-

ported westward by the African Easterly Jet, constituting great plumes that extend across the Atlantic centered around 15° N (*Cuesta et al.*, 2009).

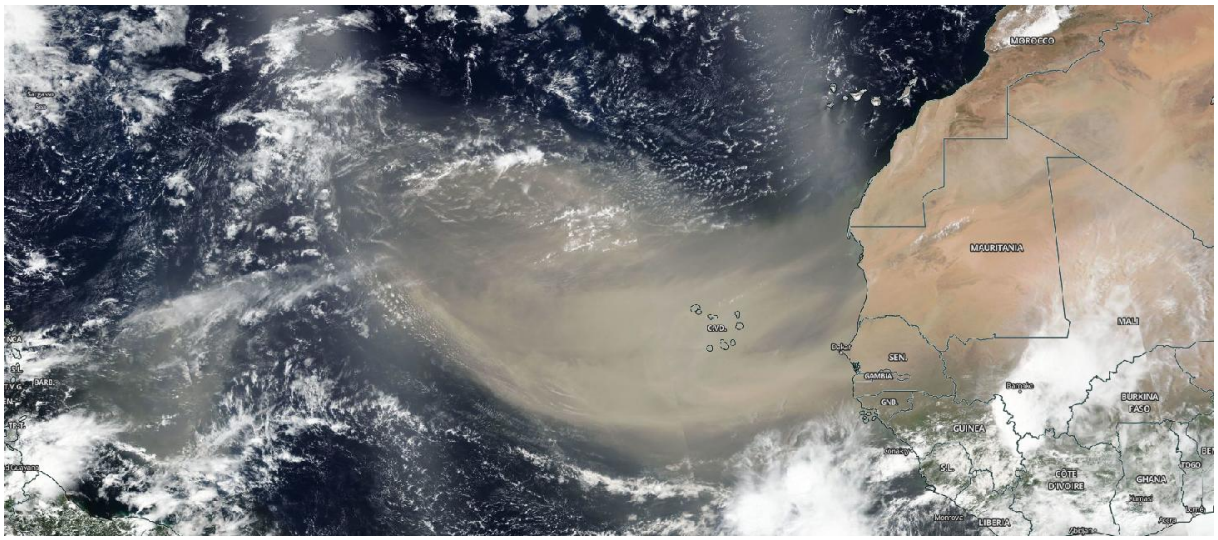

Figure 3.1: A record-breaking Saharan dust plume on June 17, 2020. Source: *NASA*.

The greatest proportion of atmospheric dust is deposited, however, in winter and early spring due to greater dust entrainment in lower levels of the atmosphere (*Yu et al.*, 2019). In the summer, tropical rains modulate much of Atlantic deposition, while other seasons are dominated by dry deposition (*van der Does et al.*, 2020). Because wet deposition is so efficient, greater dust deposition is typically recorded south of the observed dust plume due to precipitation at the southern edge of plumes associated with the Intertropical Convergence Zone (*Yu et al.*, 2019).

3.1 Data

3.1.1 Atmospheric Dust

Particles in the atmosphere absorb and scatter light, effectively blocking sunlight from reaching the ground. Aerosol optical depth (AOD) is a measure of how much sunlight is prevented from reaching the ground by aerosol particles. Greater AOD corresponds with higher aerosol

concentrations. Atmospheric dust concentrations are inferred by isolating the dust contributions to AOD, called dust optical depth (DOD). DOD can be measured from the ground using sun photometers and from space using spectroradiometers aboard satellites. Ground observation networks and remote observations work in tandem to produce a coherent global picture of aerosol dust.

ModIs Dust AeroSol

Here, we use ModIs Dust AeroSol (MIDAS), a dust optical depth (DOD) dataset (*Gkikas et al.*, 2021). DOD is a measure of how much dust is present in the atmospheric column, with greater aerosol dust concentration corresponding to higher DOD. MIDAS has high spatial and temporal coverage, with daily observations at $0.1^\circ \times 0.1^\circ$ resolution from 2003 - 2017 (Figure 3.2). This data was generated by combining satellite aerosol optical depth retrievals from the MODIS-Aqua instrument with DOD-to-AOD ratios from the Modern-Era Retrospective analysis for Research and Application version 2 (MERRA-2). MIDAS complements and expands upon existing DOD datasets by providing coverage over both continental and ocean surfaces at fine resolution, unlike the *Ginoux et al.* (2012) dataset, which has DOD at the same resolution limited to continental surfaces, or the *Voss and Evan* (2020) dataset, which has global DOD at coarse $1^\circ \times 1^\circ$ resolution. The accuracy of MIDAS was tested with ground-based observations from the AEronet RObotic NETwork (AERONET) (*Holben et al.*, 1998). Globally, MIDAS performs strongly, as it is well-correlated with AERONET observations (R=0.89). Over our regions of interest, North Africa and the tropical North Atlantic, there is even higher correlation (up to R=0.98).

Satellite measurements are spatially incomplete day-to-day due to measurements covering narrow areal swaths and obstructions to measurements, like clouds. For complete spatial coverage and standard temporal scale with our other datasets, we calculated monthly averages from the daily MIDAS observations. For each grid cell, we summed all DOD observations in each month and divided that sum by the number of observations.

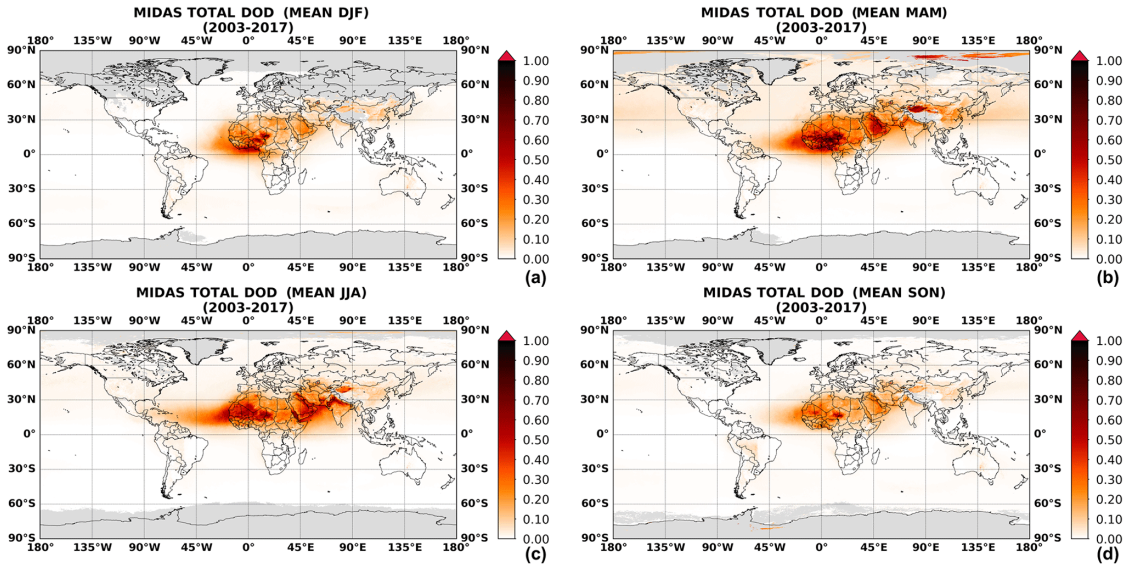

Figure 3.2: MIDAS total DOD for Northern Hemisphere (a) winter (December, January February), (b) spring (March, April, May), (c) summer (June, July, August), and (d) autumn (September, October, November). From *Gkikas et al.* (2021).

3.1.2 ERA5 Reanalysis Meteorology

For wind data, we use the ERA5 global reanalysis from the European Centre for Medium-Range Weather Forecasts (*Hersbach et al.*, 2020). Reanalysis assimilates past weather models and observations to generate a physically consistent global picture of hourly meteorology (Figure 3.3). We use monthly averaged values for zonal (east-west) and meridional (north-south) winds at 10 m above ground level and at the 850 hPa pressure level. Consistent with convention, we call the east-west component of winds U and the north-south component V. The 10-m winds best represent lofting of dust at the surface, while 850-hPa winds are a balanced representation of surface lofting along with atmospheric transport that occurs at higher altitudes. We also include wind speed in our analysis, defined as $\mathrm{W} = \sqrt{\mathrm{U}^2 + \mathrm{V}^2}$.

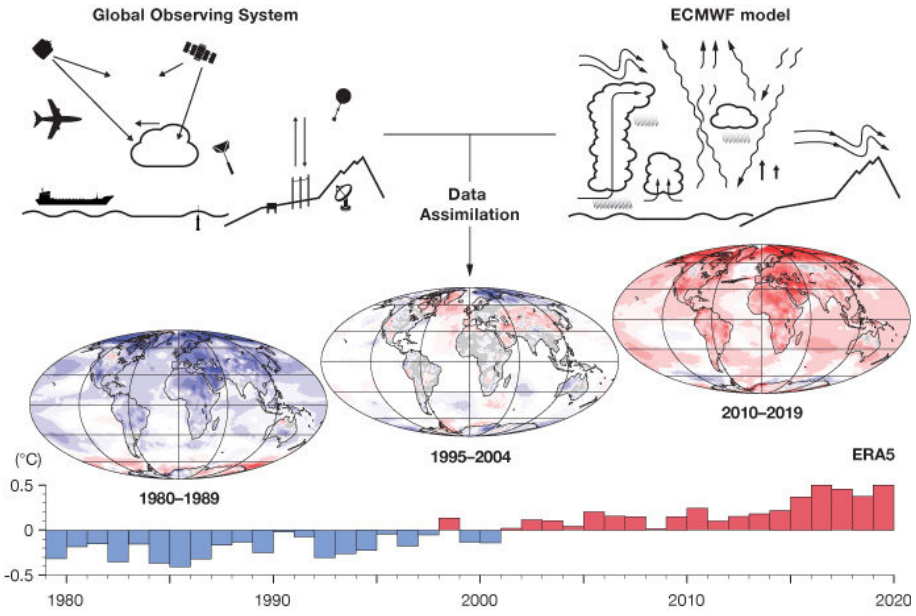

Figure 3.3: A schematic of the reanalysis process. Source: *European Centre for Medium-Range Weather Forecasts*.

3.2 Methods

3.2.1 Discerning Dust Provenance with HYSPLIT

We determine the provenance of dust arriving at the deposition sites by calculating 5-day back trajectories using the Hybrid Single-Particle Lagrangian Integrated Trajectory (HYSPLIT) model (*Stein et al.*, 2015). HYSPLIT is among the most frequently used transport and dispersion models in atmospheric sciences, and back-trajectory analysis to determine the origin of air masses is one of the most common model applications.

We calculate 24 ensemble 5-day back trajectories weekly (weeks 1 - 4 of each month) for each site over its sampling period, using Global Data Assimilation System (GDAS) meteorology. Because HYSPLIT back-trajectories do not perform well under 300 m, we ran trajectories arriving at 400 m above sea level, consistent with *Skonieczny et al.* (2013). HYSPLIT output was displayed on the Real-time Environmental Applications and Display

sYstem (READY) (*Rolph et al.*, 2017). With these transport pathways, we visually determine a dust provenance region for the nine sites so that we can compare dust over that region to deposition.

3.2.2 DOD to Dust Deposition Relationship

We evaluate the relationship between average DOD over the provenance region and deposition at each site by plotting DOD vs deposition and DOD×850-hPa wind speed (W850) vs deposition. We chose to use winds at the 850 hPa level because they balance representing surface lofting and atmospheric transport. Both DOD and W850 are averaged within the provenance region we define using HYSPLIT. As a flux, DOD×W850 matches the dimensions of dust deposition flux, but we also consider DOD alone for simplicity and to compare performance. We then assess the relationships with ordinary least squares regressions.

3.3 Results

3.3.1 Dust Provenance

There was remarkable coherence among provenance regions determined from the HYSPLIT back-trajectory calculations for all sites. Greatest variation in trajectories occurred in late summer and early fall when the West African monsoon strengthens southwesterly winds. Even during these high monsoonal wind periods, however, there was still sufficient input from the typical area in Northwest Africa. Some examples of HYSPLIT runs for site CBi-11 are in Figure 3.4. We chose a fixed box for all seasons throughout the year: 20° N to 35° N and 0° W to 18.5° W. We will hereafter refer to DOD over this area as "provenance DOD."

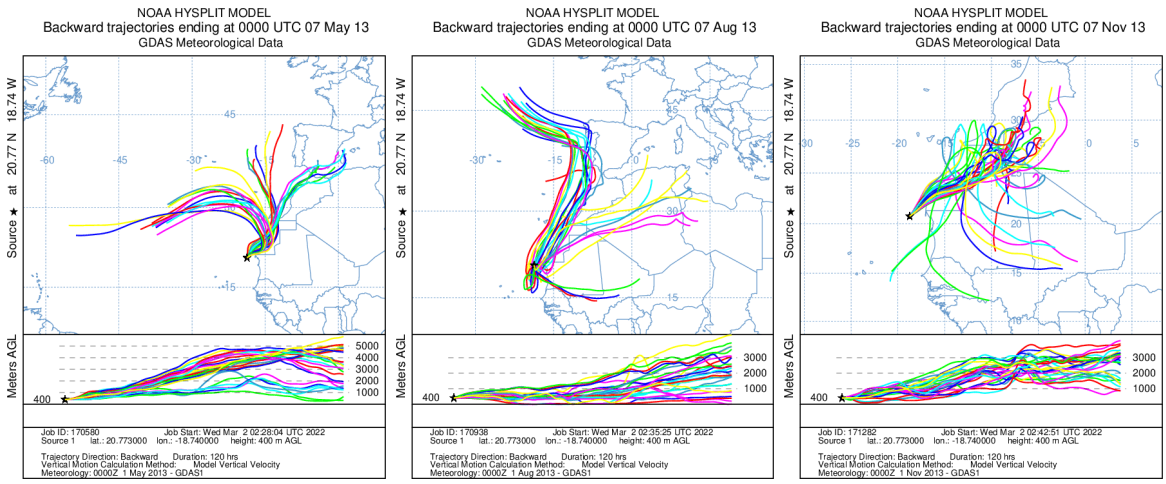

Figure 3.4: Sample HYSPLIT 5-day back trajectories for the location of site CBi-11 from May, August, and November 2013.

3.3.2 Relating Provenance DOD to Deposition Flux

We find that provenance DOD and deposition flux have a tenuous relationship for most sites. DOD×W850 had weaker correlations than DOD vs deposition, so we present analysis on the DOD vs deposition relationship. For the regressions of DOD vs deposition flux, we include R^2 and deposition coefficient values with bootstrapped 95% confidence intervals in Table 3.1. Sites M1, M2, M3, M4, and CBi-11 have significant relationships, as the 95% confidence bounds for their deposition coefficients do not cross zero. Scatter plots with their lines of best fit are in Figure 3.5. Scatter plots of DOD vs deposition for all sites are included in the Appendix (Figure A.1).

These results are not surprising given the sporadic seasonalities of deposition while DOD has a much more consistent interannual seasonal pattern peaking in summer. Therefore, it is unsurprising that only sites with peak deposition in the summer correlate with provenance DOD. Altitude of dust transport is likely the missing component to distinguishing stronger relationships between DOD and deposition flux.

Site	R^2	Depo Coefficient (95% CI)
M1	0.547	0.0082 (0.0064, 0.0101)
M2	0.0902	0.0214 (0.011, 0.032)
M3	0.177	0.0211 (0.0006, 0.0415)
M4	0.235	0.0235 (0.0152, 0.032)
CB-24	0.00454	-0.0002 (-0.0019, 0.0015)
CBi-11	0.317	0.0006 (0.0001, 0.0012)
CBi-12	0.0585	-0.0003 (-0.0012, 0.0006)
CV3	0.0134	-0.001 (-0.0034, 0.0013)
Mbour	0.00607	0.0001 (-0.0001, 0.0003)

Table 3.1: R^2 and coefficient relationships between deposition and DOD with 95% bootstrapped confidence bounds. Five sites have coefficients that are statistically significant: M1, M2, M3, M4, and CBi-11.

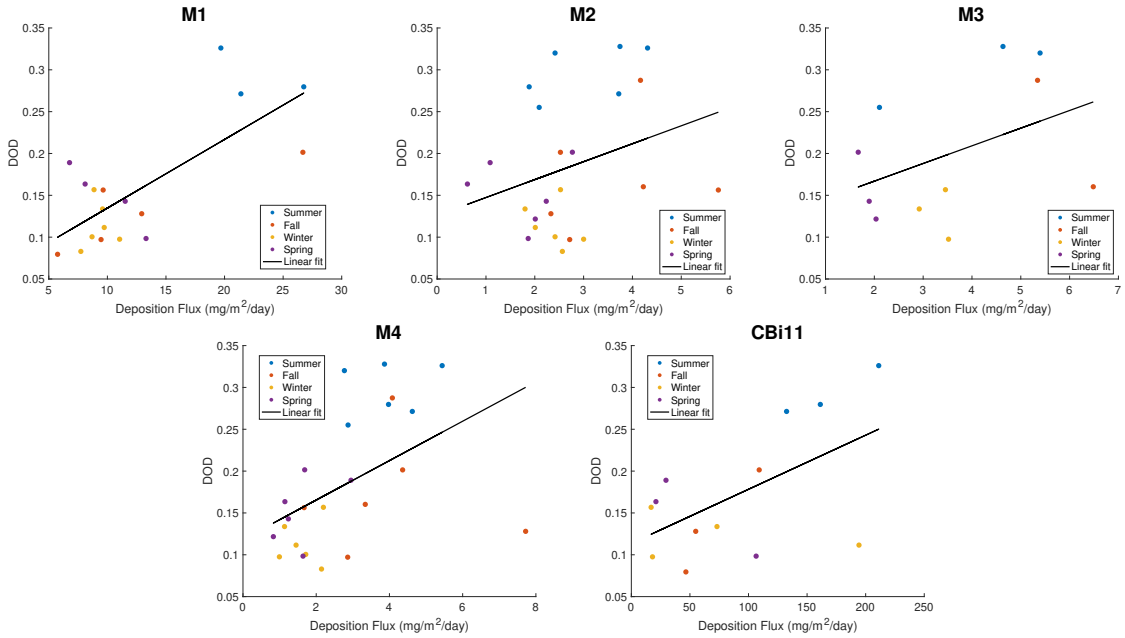

Figure 3.5: Provenance DOD vs dust deposition flux for sites with a significant relationship at the 95% confidence level. Points are separated by season: summer in blue, fall in orange, winter in yellow, and spring in purple. Plots for other sites are included in Appendix (Figure A.1).

3.4 Discussion

That some of the deposition sites (five of nine) have a significant relationship with provenance DOD lends some support to the notion that it is possible to infer dust deposition from dust concentration. However, the generally weak relationships between DOD and deposition affirm the complex relationship between offshore deposition and regional dust concentrations. Only deposition sites that happened to record peak deposition in summer correspond well with provenance DOD. This distinction is critical to bear in mind while judging the fidelity of dust as an aridity proxy: more dust present in the atmosphere at a certain time does not necessarily mean that greater dust will be recorded in marine sediments. The tenuous relationships between atmospheric dust and offshore deposition prevent simple interpretation of aeolian dust deposition.

These relationships are tenuous because the regular seasonal cycle of aerosol dust is not shared among deposition records. Better resolving what drives seasonal variations in deposition would help clarify this relationship. Once again, having deposition records that last several more years would help us to address this major seasonality problem.

Our simple approach is a quick check on the correspondence of ambient "dustiness" and deposition, and it shows that atmospheric dust is not a strong determinant of deposition alone. We could improve this model by accounting for other factors known to influence dust deposition like vertical dust distribution, but this quickly escalates the complexity of the problem and is beyond the scope of this work.

Chapter 4

On the Relationship of Atmospheric Dust and Land Surface Characteristics

So far, we have found that deposition flux is highly heterogeneous through space and time, and that there are dubious linkages between atmospheric dust concentrations and deposition flux. We now move to explore what dust concentrations might tell us about land surface characteristics.

4.1 Data

Once again, we draw from MIDAS for atmospheric DOD and ERA5 for 10-m winds to characterize atmospheric conditions near the surface. To include vegetation in our analysis as a proxy for aridity, we use the normalized difference vegetation index.

4.1.1 Normalized Difference Vegetation Index

The normalized difference vegetation index (NDVI) indicates vegetation presence and health. NDVI is a ratio between the reflectance of red and near-infrared (NIR) light:

$$\text{NDVI} = \frac{\text{NIR} - \text{RED}}{\text{NIR} + \text{RED}}$$

Healthy plants absorb strongly in the visible red and reflect near-infrared. NDVI values range from -1 to +1, where negative values correspond to an absence of vegetation (Figure 4.1). Higher NDVI corresponds with greater chlorophyll abundance and energy absorption

which influence plant growth through photosynthesis (*Myneni et al.*, 1995).

Figure 4.1: A schematic interpretation of NDVI values. Source: *Earth Observing System*.

Our NDVI data comes from the MODerate resolution Imaging Spectroradiometer (MODIS) aboard the Terra satellite. We use the Collection 6 Terra MODIS monthly product MOD13C2 with a spatial resolution of $0.05^\circ \times 0.05^\circ$ (*Didan*, 2015). Figure 4.2 is an example of NDVI values throughout North Africa.

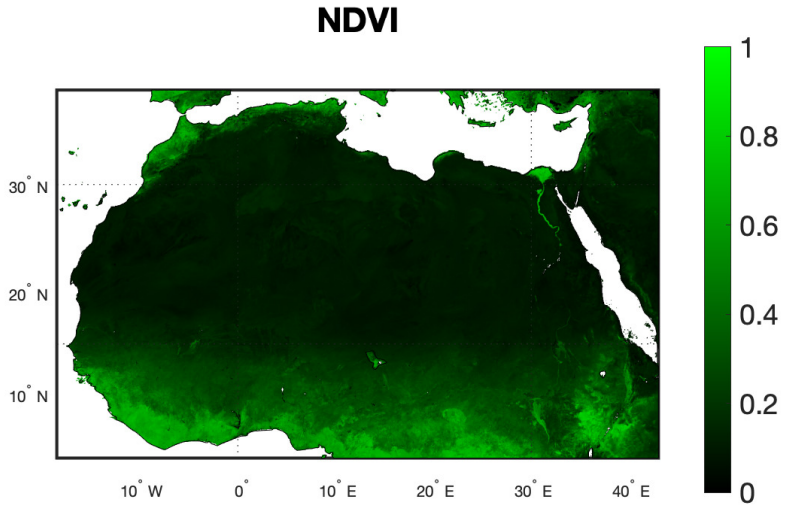

Figure 4.2: MODIS NDVI of North Africa from January 2003. Mostly unvegetated, the Sahara has NDVI close to zero. South of 15° N, a gradual fading into higher NDVI marks the desert transition to Sahelian grassland.

4.2 Methods

We separate our analysis by season to control for the strong seasonal patterns of dust, winds, and vegetation cover. Considering each season separately is advantageous because we can assess the dominant patterns during each part of the year. Seasonal separation entails averaging the observations across the three months that constitute each season for each year: December, January, February for winter; March, April, May for spring; June, July, August for summer; and September, October, November for fall. We then have a 15-year time series of the dust, wind, and vegetation fields for each season for our analysis.

4.2.1 Composite Maps

For a spatially-resolved view of favorable vegetation and wind conditions for higher dust concentrations, we construct composite maps. These maps are the result of subtracting the wind and NDVI fields associated with lowest provenance DOD from those that correspond with highest provenance DOD. For the seasonal NDVI fields, we divide each grid cell by its season's average across all 15 years in order to focus on the deviation of each grid cell from average because the high NDVI signal from the tropics would otherwise hide smaller signals from the semi-arid Sahel.

To construct the composite maps, we first identify the top and bottom 20% dusty years by season by ranking average provenance DOD and then identifying the top and bottom three years. We average the NDVI and wind fields for these two year groups to make average "dusty" and "clean" maps that reflect the vegetation and wind conditions that are favorable and least favorable to high dust concentrations. Finally, we subtract "clean" from "dusty" average maps to produce our composite map. This composite illustrates NDVI and wind conditions that are most favorable to high provenance DOD.

4.2.2 Point-to-Field Regressions

We perform seasonal point-to-field regressions of average provenance DOD with vegetation and wind fields as an additional way to visualize how dust conditions correspond with vegetation and winds. For each grid cell of the wind or vegetation field, we plot the correlation coefficient R between the time series of that grid cell with the time series of average provenance DOD. In addition to wind speed, we also construct point-to-field regression maps for the north-south (U) and east-west (V) components of wind to note directional influence of winds on dust export.

4.2.3 Linear Models

To quantify the relative influences of vegetation and winds on DOD, we calculate correlation coefficients (R) among DOD, NDVI, and winds in the dust provenance box. We perform this analysis for each season independently and for annual averages.

We will also fit a linear model for each season:

$$\text{DOD'} = \text{NDVI'} + \text{WIND'}$$

The primes indicate that we standardize all three variables to zero mean and variance of one so that we can directly compare the relative influences that each of wind and vegetation has on dust. This way, the size of the NDVI and wind coefficients are directly reflective of how much they influence DOD and are not skewed by their different scales. WIND' will be whichever wind variable (total speed, east-west component, or north-south component) predicts dust concentration well according to correlation coefficients.

We intentionally keep this model simple to evaluate the relative influences of vegetation and wind—both separated by direction and the total magnitude—to determine what factors mediate dust concentration in the region, and ultimately, what factors are more conducive to interannual dust deposition.

4.3 Results

4.3.1 Composite Maps

Given the classic paleoclimate interpretation of greater dust corresponding with lower vegetation, we would expect to see that "dusty" minus "clean" composite NDVI maps should exhibit generally negative patterns. The composite NDVI variation maps reveal an unexpected mixed signal over the Sahel for summer (Figure 4.3). Fall has a consistently negative pattern throughout the Sahel, while winter and spring do not have strong signals across the eastern side of the Sahel. Remarkably, only one of the four seasons, fall, has the negative pattern we would expect to see between vegetation and dust.

Summer's great heterogeneity along the Sahel is an especially surprising result—the season with greatest dust concentrations has the most variable NDVI patterns that correspond with dusty conditions. We explain this result by accounting for the condition which makes summers so dusty: strong surface turbulence from the West African monsoon which convectively lifts dust. Vegetation and soil moisture heterogeneity have been associated with mesoscale circulations which have been observed to trigger convection in the Sahel (*Taylor et al.*, 2010, 2011). Therefore, this spotty pattern may indicate that when these areas contrast more with each other, the mechanism by which dust is lofted is greatly enhanced. Given this phenomenon occurs during the time of year when dust lofting is greatest, it would be worthwhile to study how vegetation and soil moisture heterogeneity modulate dust export.

Composite wind maps for summer and winter both have little signal across North Africa except for northeasterly winds in the northwesternmost side of the continent (Figure 4.4). Meanwhile, fall and spring have easterlies across 25° N. Each season having some enhanced easterly wind is consistent with expectations. There is a slight westerly wind pattern across 15° N during winter, which signals that weaker easterly harmattan winds correspond with higher dust.

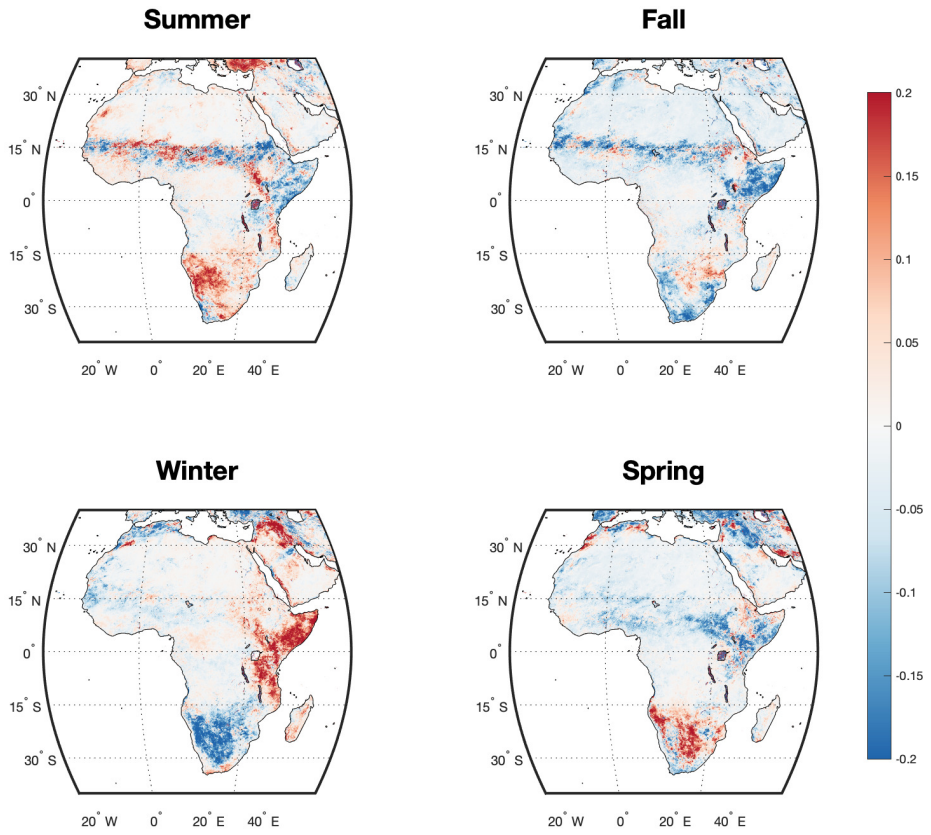

Figure 4.3: Seasonal composite "dusty" minus "clean" NDVI deviation fields. Fall shows the expected pattern of anticorrelation along the Sahel. Winter and spring do not show a strong signal across the eastern side of the Sahel. Summer has a very mixed signal across the Sahel that is very slightly positive overall.

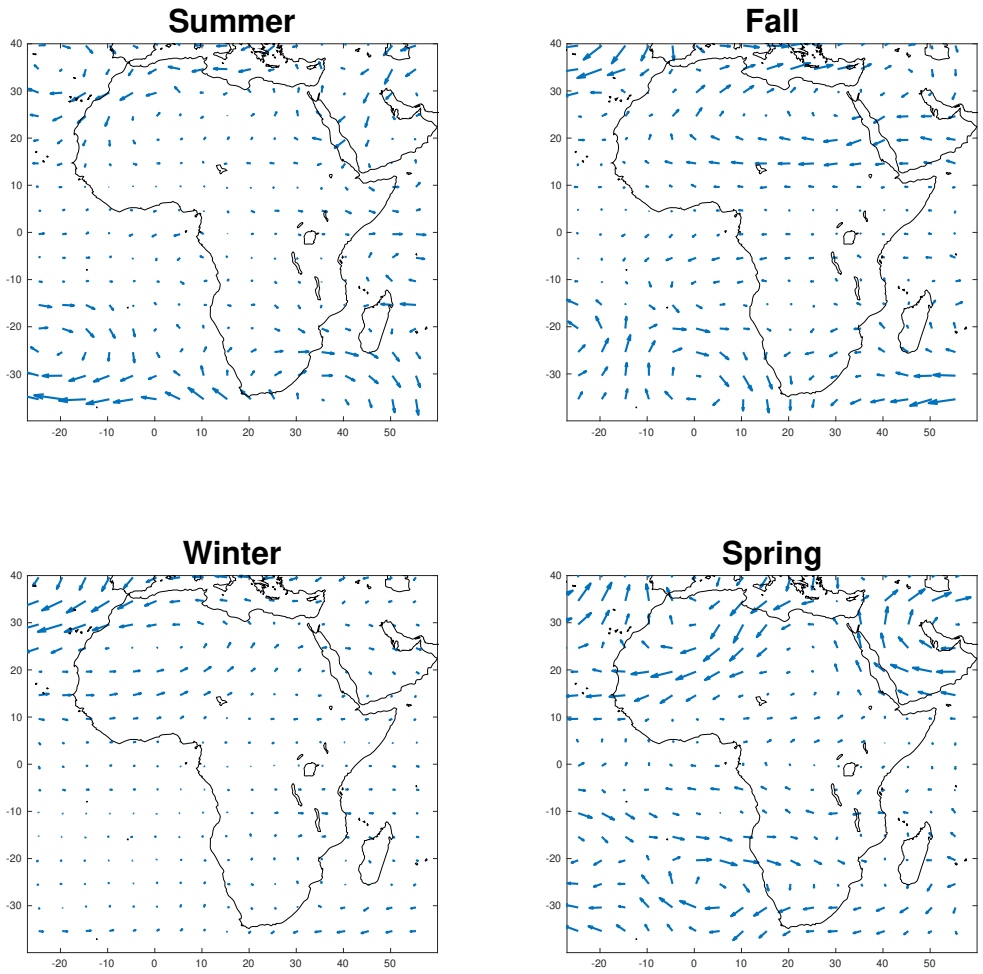

Figure 4.4: Seasonal composite "dusty" minus "clean" wind fields. Summer and winter have slight northeasterly wind patterns coinciding with the provenance DOD region. Fall and spring have an easterly wind pattern across 25° N.

4.3.2 Point-to-Field Regressions

Given the traditional dust-aridity interpretation, we expect to observe anticorrelation between provenance DOD and NDVI in North Africa. We see this expected anticorrelation in all seasons except for summer (Figure 4.5). As with the composite NDVI map, summer's correlation pattern is very mixed between positive and negative signals.

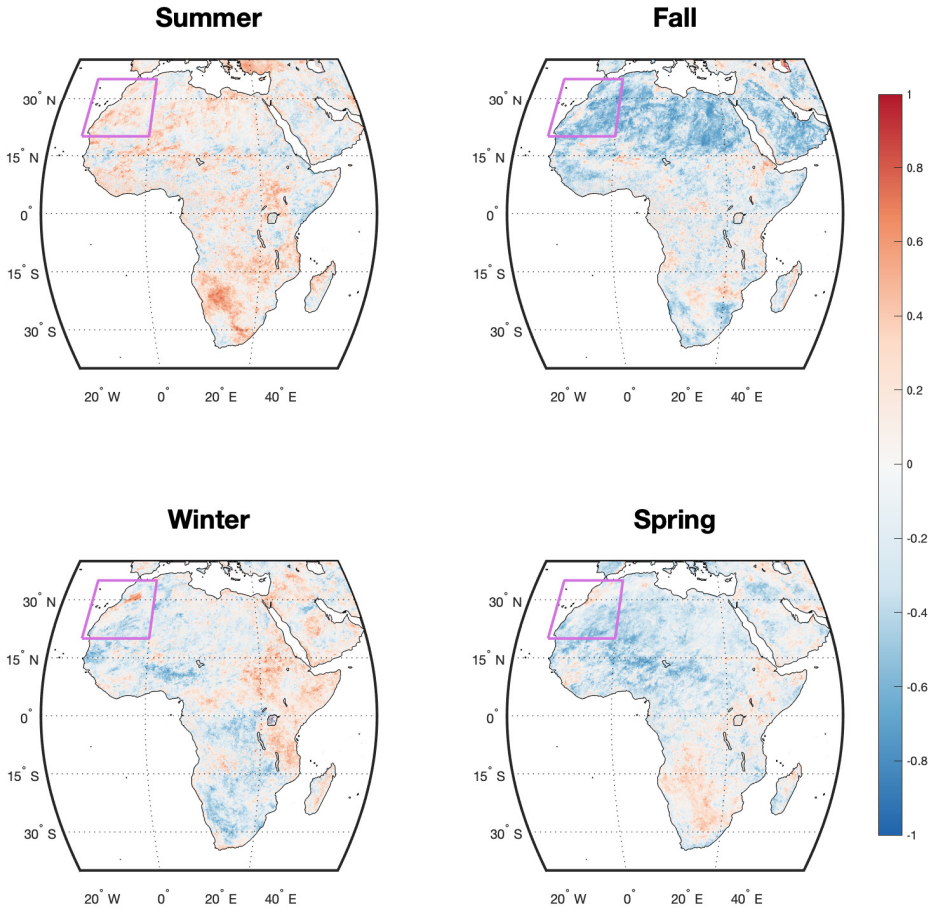

Figure 4.5: Seasonal point-to-field regressions between average provenance DOD marked by pink box and NDVI field. Summer has a mixed pattern that is slightly positive. Fall, winter, and spring have generally negative relationships which are more consistent with expectations.

We expect provenance DOD and 10-m wind speeds to be positively correlated, as higher surface wind should loft more dust. The correlation between provenance DOD and 10-m wind speeds reveal overall positive correlation across North Africa during fall and winter (Figure 4.6). Summer has a slightly negative relationship through most of Northwest Africa, and spring has a strong positive correlation band across North Africa that fades to a slightly negative relationship north of 20° N. As with NDVI, summer has a puzzling mix of positive and negative correlations across North Africa. Amidst the negative correlations, spring and

summer both have positive correlation hotspots around the Bodélé Depression, the greatest source of mineral dust in the Sahara (*Koren et al.*, 2006).

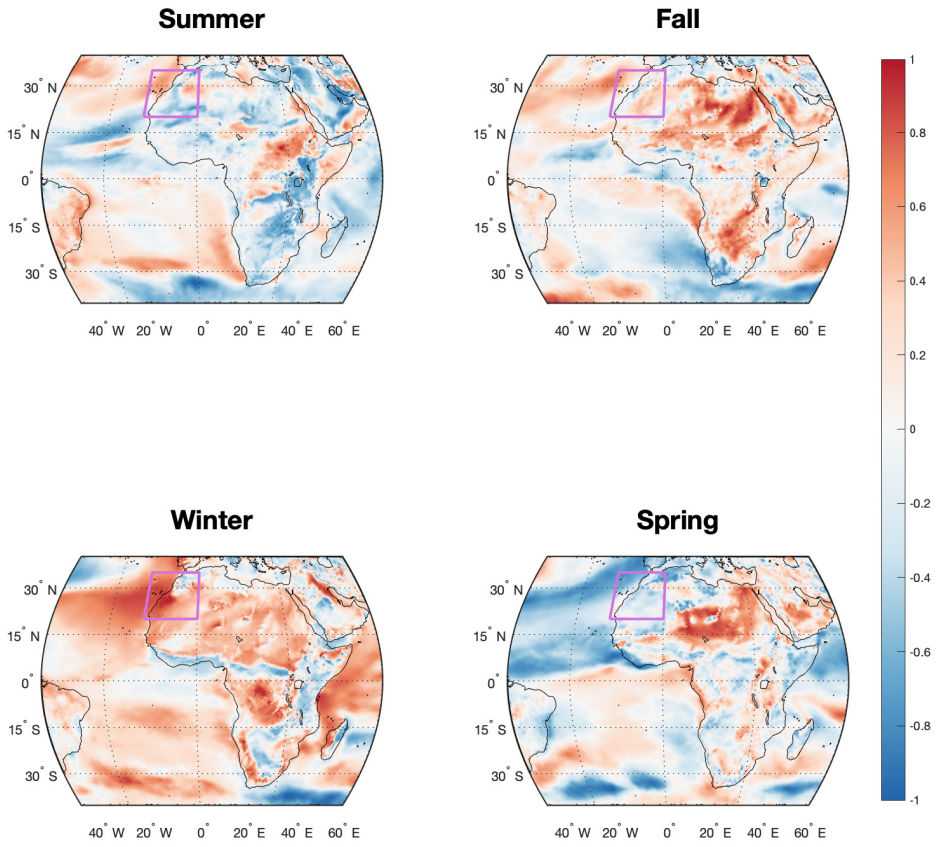

Figure 4.6: Seasonal point-to-field regressions between average provenance DOD marked by pink box and 10-m wind speed field. Fall and winter have higher DOD with higher wind speeds across most of North Africa. Spring has a mostly positive relationship with a slightly negative pattern north of 20° N. Summer has a mixed but mostly negative pattern over the region.

Now we assess the two directional components of 10-m wind. Dust is primarily transported via northeasterly winds, so we would expect to observe anticorrelation between east-west winds and provenance DOD because the west direction is negative. There is a consistent anticorrelation across Northwest Africa for all seasons except summer (Figure 4.7). Summer

has mostly anticorrelation within the provenance region, but positive correlation throughout the continent outside the box.

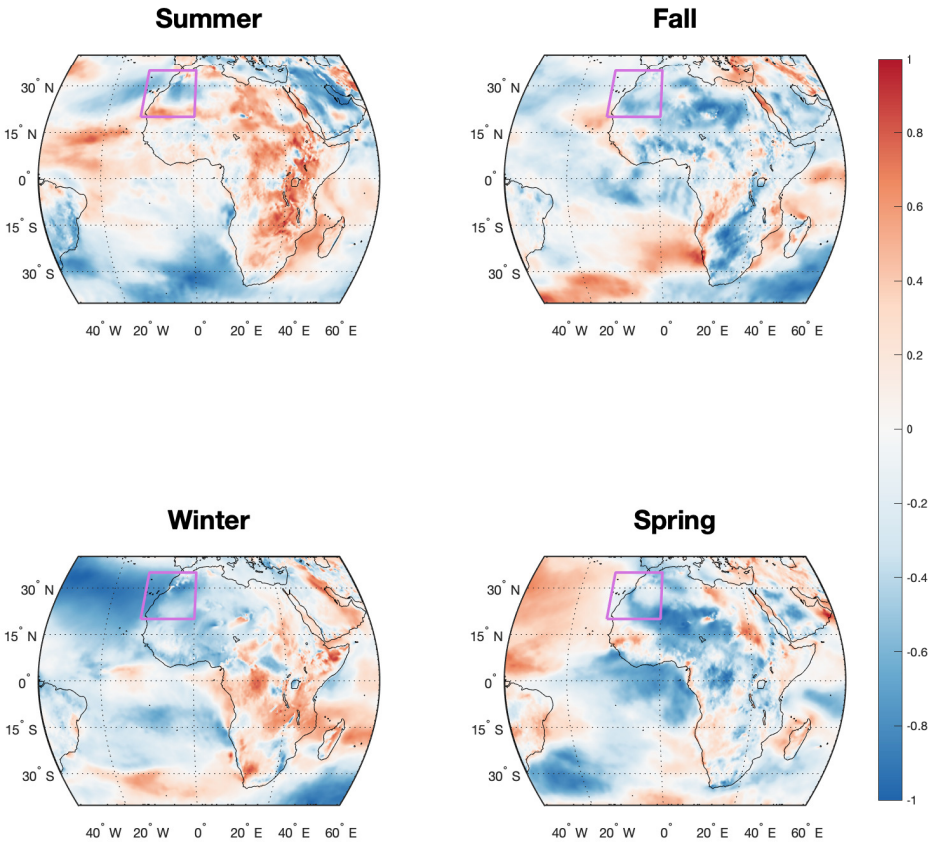

Figure 4.7: Seasonal point-to-field regressions between average provenance DOD marked by pink box and 10-m east-west wind field. East is defined as negative, so stronger westerlies are more negative. In all seasons except summer, stronger westerlies coincide with higher provenance DOD. Within the provenance box, summer has the same anticorrelation, but the pattern is weaker throughout the rest of the continent.

For north-south winds, summer and fall both have very mixed patterns across North Africa. Winter has a consistent anticorrelation pattern, while spring has anticorrelation west of 10° E and positive correlation across the rest of North Africa (Figure 4.8). Winter's anticorrelation signals a strengthened northerly component of the harmattan.

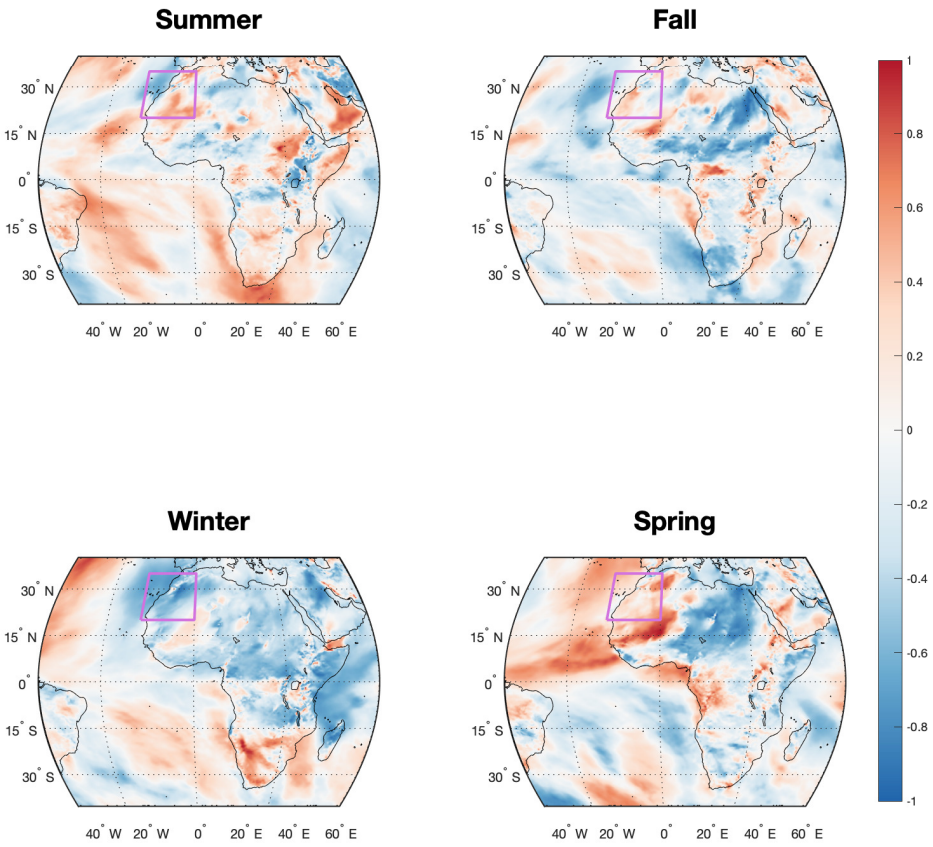

Figure 4.8: Seasonal point-to-field regressions between average provenance DOD marked by pink box and 10-m north-south wind field. Summer and fall have very mixed patterns. Winter has a pervasive anticorrelation across North Africa indicating a stronger northerly component of the harmattan. Spring has positive correlation along the easternmost side of North Africa and reverses to negative correlation west of 10°E.

Note that all the wind correlation maps have higher correlations than the NDVI correlation maps. Winds having stronger correlation with dust than NDVI is consistent with modern observations in the literature which find that Saharan dust has stronger correspondence with wind than with vegetation (*Kim et al.*, 2017).

	NDVI	W10	U10	V10
Summer DOD	0.2684	0.2993	-0.2964	-0.1688
Fall DOD	-0.6896	0.1064	-0.2241	0.0728
Winter DOD	-0.1655	0.6506	-0.5403	-0.5881
Spring DOD	-0.0589	-0.4087	-0.3371	0.4652
Annual DOD	-0.0578	-0.0911	-0.2699	0.3567

Table 4.1: Correlation coefficients (R) between DOD and NDVI, 10-m wind speed, and components of 10-m wind.

4.3.3 Linear Models

The point-to-field regressions and composite maps provide a qualitative foundation for our assessment of what factors correspond with higher dust conditions. We now move to a quantitative analysis of the relative influence of wind and vegetation on dust in the provenance region, beginning with assessing correlations among DOD, NDVI, and 10-m winds.

Table 4.1 contains correlation coefficients between DOD, NDVI, and 10-m winds within the provenance region. Notably, summer is the only season that has a counterintuitive positive correlation with NDVI. For all other seasons and for the annual average, NDVI anti-correlates with DOD. W10 and U10 correlate with DOD about equally well; W10 performs better in winter and spring while U10 performs better for annual and fall. Thus, we will run linear models predicting DOD with both NDVI/W10 and NDVI/U10 by season and by annual averages.

In the wind speed models (Table 4.2), the fall and winter models were significant at the 5% level with R^2 values of 0.478 and 0.425. Summer and spring have very weak relationships (R^2 of 0.139 and 0.192), and the annual model has practically no relationship ($R^2 = 0.015$). Summer is the only season that has a positive relationship between NDVI and DOD. During summer, wind speed and NDVI also have approximately equal influence on DOD. In winter and spring, wind speed is a stronger predictor of DOD; in fall, NDVI has a larger influence than wind.

DOD' ~ NDVI' + W10'				
	R^2	**p-value**	**NDVI' (p-value)**	**W10' (p-value)**
Summer	0.139	0.406	0.226 (0.420)	0.263 (0.351)
Fall	0.478	0.020	-0.702 (0.007)	-0.054 (0.806)
Winter	0.425	0.036	-0.040 (0.862)	0.642 (0.014)
Spring	0.192	0.278	-0.163 (0.553)	-0.447 (0.120)
Annual	0.015	0.916	-0.081 (0.788)	-0.109 (0.719)

Table 4.2: Models that use wind speed. Seasonal and annual linear model R^2, p-values, and coefficients for NDVI' and W10' with each of their p-values.

DOD' ~ NDVI' + U10'				
	R^2	**p-value**	**NDVI' (p-value)**	**U10' (p-value)**
Summer	0.146	0.388	0.241 (0.385)	-0.272 (0.323)
Fall	0.477	0.021	-0.680 (0.009)	-0.034 (0.878)
Winter	0.293	0.125	-0.031 (0.904)	-0.532 (0.055)
Spring	0.166	0.477	-0.049 (0.860)	-0.336 (0.240)
Annual	0.0729	0.635	0.008 (0.978)	-0.272 (0.361)

Table 4.3: Models that use east-west wind. Seasonal and annual linear model R^2, p-values, and coefficients for NDVI' and U10' with each of their p-values.

The models that use east-west winds (Table 4.3) perform very similarly to the wind speed models, with the same relative influences of wind and NDVI on dust by season (about even in summer, NDVI stronger in fall, and wind stronger in winter and spring). The only notable difference is that the winter model is weaker and insignificant at 5% level for these models. For a visual example of model performance, plots of predicted and observed DOD for all seasons and the annual average for the U10 models are in Figure 4.9.

Inasmuch as the wind and NDVI coefficients are statistically identifiable, winds are much stronger influences on dust than vegetation in winter and spring. Both winds and vegetation have equal influence on dust in the summer. During fall, vegetation has greater control on dust.

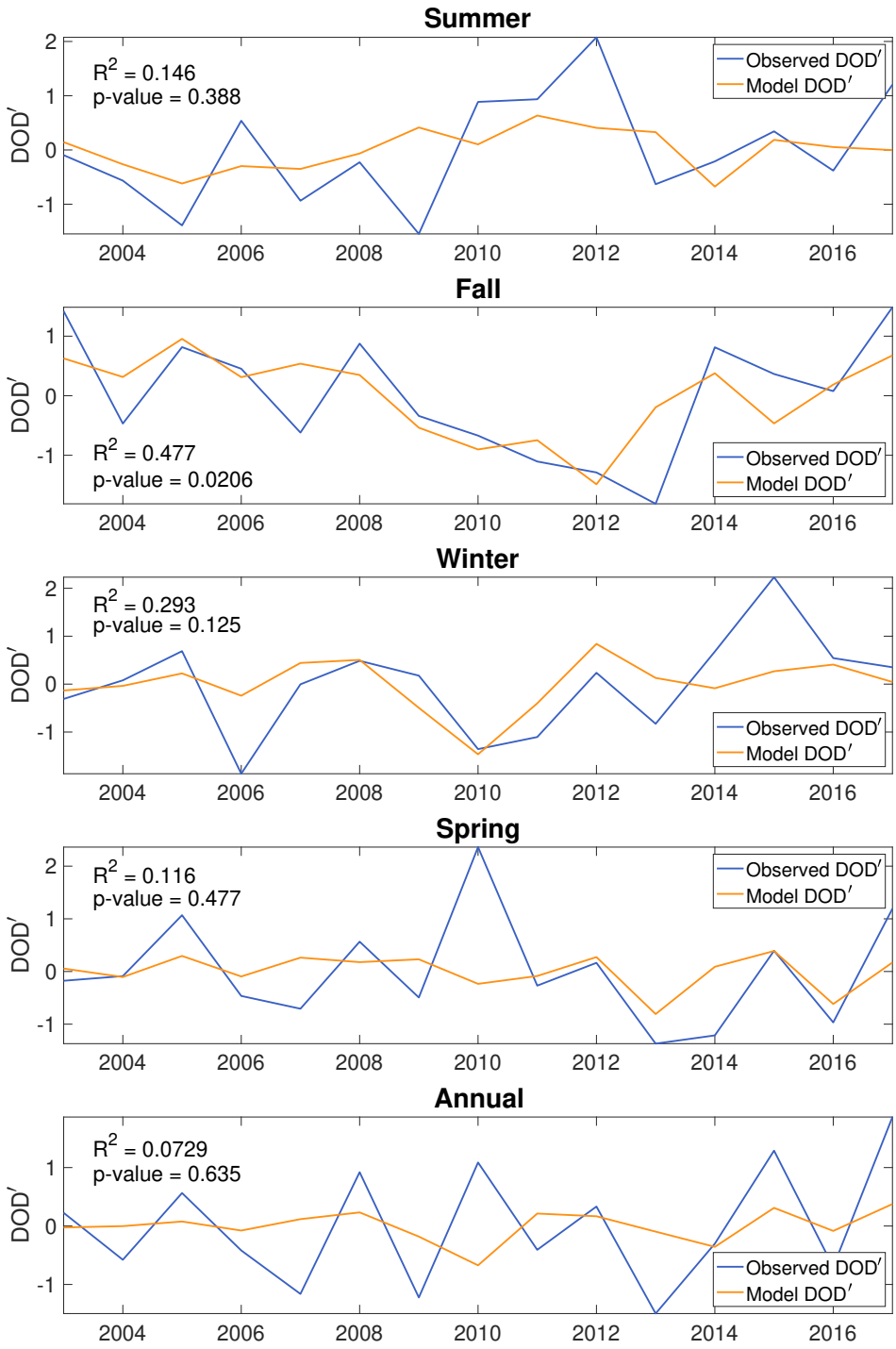

Figure 4.9: Observed and model-predicted DOD for all seasons and the annual average for predictors NDVI' and U10'. Only the fall model is statistically significant at the 5% level.

4.4 Discussion

Our maps and models show that wind and vegetation controls on dust are highly variable season to season. Most studies that consider competing influences on dust emission only consider interannual variations (e.g., *Kim et al.*, 2017), but it is important to separate seasonal effects because the system's behavior is so season-dependent. The weakness of the annual-average models is surprising but indicates that the different seasonal behaviors average to a very mixed, poor signal.

Our provenance box is in a very arid region of the Sahara, and our results would be different if we focused study on the semi-arid Sahel to the south. *Kim et al.* (2017) performed a similar analysis on the Sahel and still found winds to be the dominant interannual control on dust emissions. We also note that this is a basic evaluation of how dust, vegetation, and wind correspond within the provenance area alone that neglects dust that comes from outside the region.

Given how differently dust behaves due to wind and vegetation influences according to season, it is imperative to understand what determines which seasons experience the most dust deposition year to year. The season during which most deposition occurs dictates how we interpret changes in dust deposition in relation to wind and aridity.

In our dust deposition records, we observed the most deposition occurring across sites during summer and late winter/early spring. Fall was the only season that saw greater NDVI influence on dust than winds. Given fall also records the least dust deposition of all seasons, this NDVI signal shrinks in the record relative to inputs from other seasons. Therefore, winds seem to have greater influence on dust deposition than vegetation. The surface winds reflect variations in the trade winds and Hadley circulation, so aeolian dust appears to be deeply tied to large-scale tropical circulation variability.

Overall, aeolian dust flux seems to be more a proxy of tropical circulation strength than of aridity. Wind strength is most often proxied with dust grain size distribution—coarser

particle sizes indicate stronger wind periods (e.g., *Matthewson et al.*, 1995). Given that modern observations show that winds have a dominant influence on dust export, grain size and total dust flux should be taken together to be wind strength proxies.

Wind may also appear to be the major control on dust because it has much higher interannual variability than vegetation. The significance of interannual variation shrinks when considering that paleo records have time scales on the order of centuries to millennia. At long time scales, vegetation may undergo changes at the same scale as winds, significantly increasing the effect of greenness on dust export. Therefore, our examination of interannual variability in a slim 15-year period cannot refute the traditional paleo interpretation. Rather, our results confirm that what is observed in the modern system does not lend much support to the dust-aridity direct connection established in paleoclimate literature. Our work underscores the tension that exists between what is observable in the modern system and inferences drawn in paleoceanographic records.

Chapter 5

Further Discussion and Conclusions

The ultimate goal of a project attempting to calibrate climatic interpretations of past dust deposition would be a model that resolves the physics of dust lofting, transport, and deposition in a framework which accurately accounts for seasonal variations. This model would be very complicated, however, and accounting for all the physics at play in a complete model is not strictly best for clean paleoclimatic inferences. There will always be a sea of influences that affect proxy interpretation, and an ideal model balances such complexity with interpretability. The analysis we conducted was necessarily limited by the brevity and scarcity of real deposition records. Although our analysis is not as complete as would be ideal, there is still great utility in our findings.

Our simple approach reveals that wind and vegetation controls on dust are highly variable according to season. During fall, vegetation had a greater influence on aerosol dust. During winter and spring, wind dominated vegetation's effect on dust. During summer, wind and vegetation had about equal influence on aerosol dust. Interannually, the relationship between wind, vegetation, and dust was unclear. If we weigh our season-dependent results according to our observations that highest dust flux in the records tended to occur during summer and late winter/early spring, we surmise that wind makes the dominant appearance in the dust record. Summer was also the only season during which vegetation positively correlated with dust. This positive correlation along with summer's heterogeneous vegetation patterns that corresponded with highest dust suggest that summer's convective dust lofting is intensified by enhanced, scattered vegetation cover.

Because our deposition data too was sparse to discern a continuous land-to-ocean signal,

we had to segment our analysis into distinct land-to-air and air-to-ocean pieces. In some ways, segmenting dust's journey as we did underscores the degree to which the classic interpretation of dust flux neglects the fundamental complexity of dust dynamics; that the signals we detected are faint even when simply tracing these steps independently reveals the many places when simple interpretations can be overcome by noise and unaccounted-for mechanisms. We could improve upon this preliminary work by integrating dust emission and deposition models which would provide sufficient spatio-temporal resolution to produce a continuous perspective on dust's land-to-sea journey.

In summary, we observed that aeolian dust flux in Northwest Africa seems to be more a proxy of tropical circulation strength than of continental vegetation during our studied period. These findings do not lend support to the traditional interpretation of aeolian dust flux. The weaknesses of these relationships we find emphasize the great need for more observational data and further work to make proper sense of this prominent paleoclimate proxy.

Appendix A

Supplemental Figures

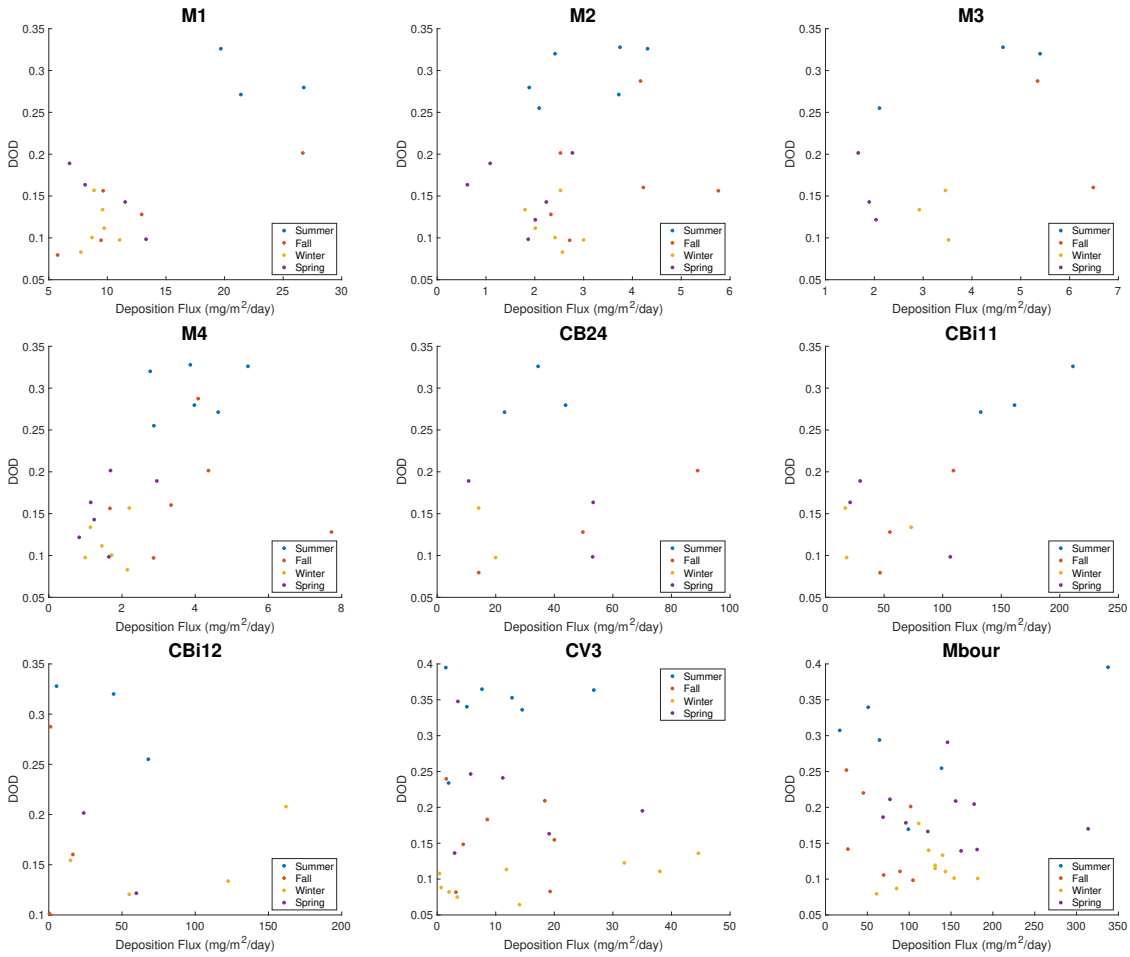

Figure A.1: Provenance DOD vs dust deposition flux for all sites.

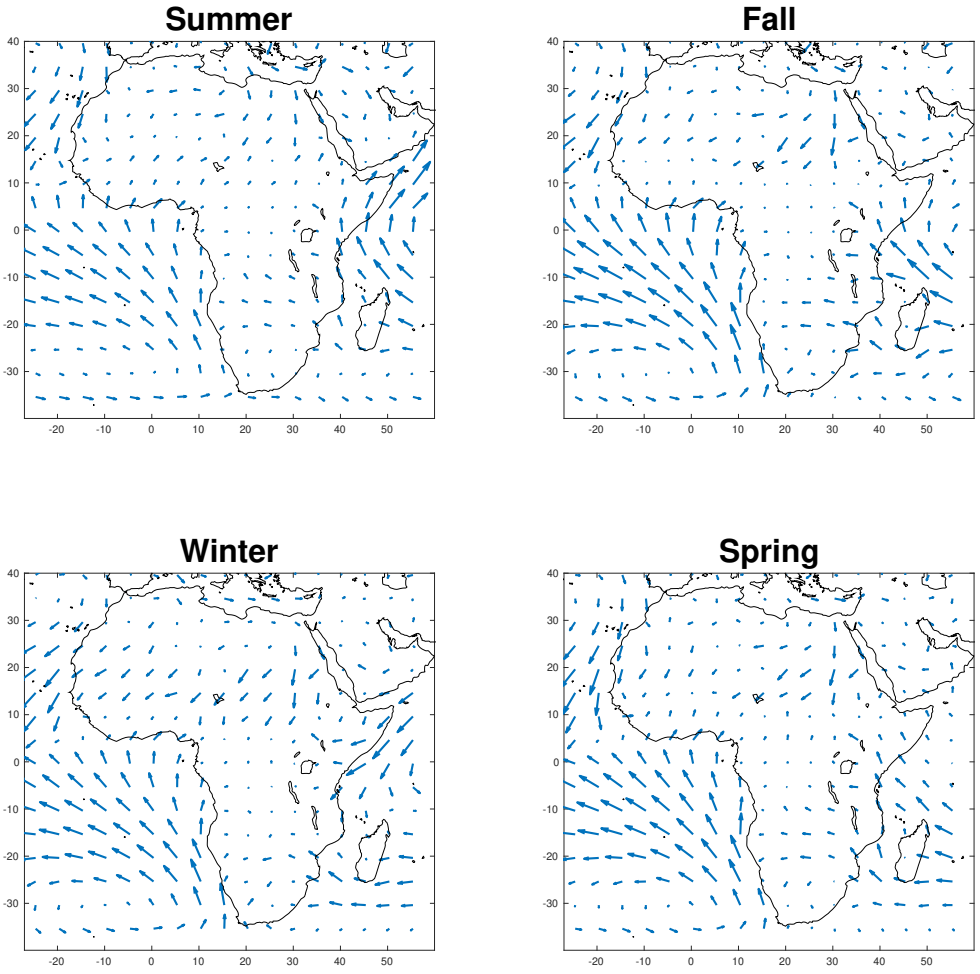

Figure A.2: Seasonal 10-m African wind climatology from ERA5.

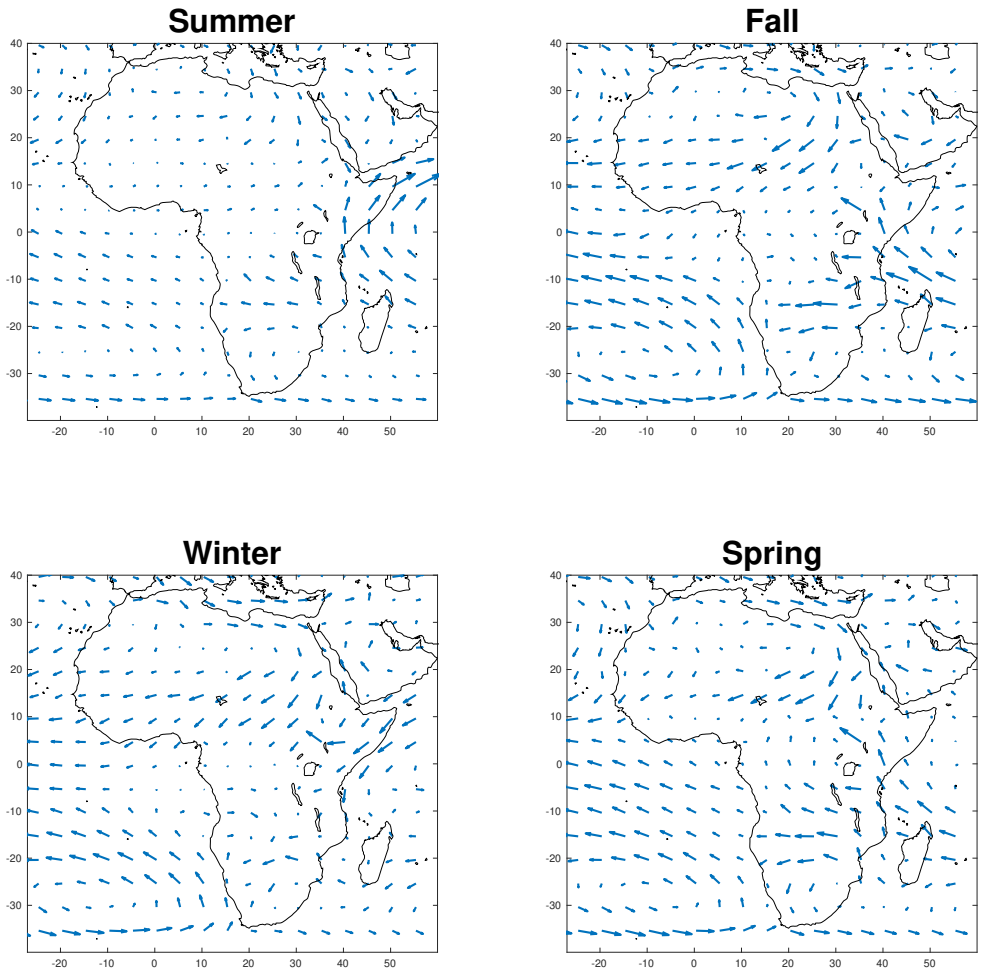

Figure A.3: Seasonal African 850 hPa wind climatology from ERA5.

References

Blome, M. W., A. S. Cohen, C. A. Tryon, A. S. Brooks, and J. Russell (2012), The environmental context for the origins of modern human diversity: a synthesis of regional variability in african climate 150,000–30,000 years ago, *Journal of human evolution*, *62*(5), 563–592.

Brooks, N. (2006), Cultural responses to aridity in the middle holocene and increased social complexity, *Quaternary International*, *151*(1), 29–49.

Calvin, W. H. (2003), *A brain for all seasons: Human evolution and abrupt climate change*, University of Chicago Press.

Chauvin, F., R. Roehrig, and J.-P. Lafore (2010), Intraseasonal variability of the saharan heat low and its link with midlatitudes, *Journal of Climate*, *23*(10), 2544–2561.

Cuesta, J., J. H. Marsham, D. J. Parker, and C. Flamant (2009), Dynamical mechanisms controlling the vertical redistribution of dust and the thermodynamic structure of the west saharan atmospheric boundary layer during summer, *Atmospheric Science Letters*, *10*(1), 34–42.

Cullen, H. M., P. B. Demenocal, S. Hemming, G. Hemming, F. H. Brown, T. Guilderson, and F. Sirocko (2000), Climate change and the collapse of the akkadian empire: Evidence from the deep sea, *Geology*, *28*(4), 379–382.

deMenocal, P., J. Ortiz, T. Guilderson, J. Adkins, M. Sarnthein, L. Baker, and M. Yarusinsky (2000), Abrupt onset and termination of the african humid period:: rapid climate responses to gradual insolation forcing, *Quaternary science reviews*, *19*(1-5), 347–361.

deMenocal, P. B. (2004), African climate change and faunal evolution during the pliocene–pleistocene, *Earth and Planetary Science Letters*, *220*(1-2), 3–24.

Didan, K. (2015), Mod13c2 modis/terra vegetation indices monthly l3 global 0.05 deg cmg v006, *NASA EOSDIS Land Processes DAAC*, *10*, 2015.

Drake, N. A., R. M. Blench, S. J. Armitage, C. S. Bristow, and K. H. White (2011), Ancient watercourses and biogeography of the sahara explain the peopling of the desert, *Proceedings of the National Academy of Sciences*, *108*(2), 458–462.

Ehrmann, W., G. Schmiedl, S. Beuscher, and S. Krüger (2017), Intensity of african humid periods estimated from saharan dust fluxes, *PloS one*, *12*(1), e0170,989.

Figgis, B., B. Guo, W. Javed, S. Ahzi, and Y. Rémond (2018), Dominant environmental parameters for dust deposition and resuspension in desert climates, *Aerosol Science and Technology*, *52*(7), 788–798.

Forman, S. L., D. K. Wright, and C. Bloszies (2014), Variations in water level for lake turkana in the past 8500 years near mt. porr, kenya and the transition from the african humid period to holocene aridity, *Quaternary Science Reviews*, *97*, 84–101.

Friese, C. A., J. A. Van Hateren, C. Vogt, G. Fischer, and J.-B. W. Stuut (2017), Seasonal provenance changes in present-day saharan dust collected in and off mauritania, *Atmospheric Chemistry and Physics*, *17*(16), 10,163–10,193.

Gasse, F. (2002), Diatom-inferred salinity and carbonate oxygen isotopes in holocene waterbodies of the western sahara and sahel (africa), *Quaternary science reviews*, *21*(7), 737–767.

Ginoux, P., J. M. Prospero, T. E. Gill, N. C. Hsu, and M. Zhao (2012), Global-scale attribution of anthropogenic and natural dust sources and their emission rates based on modis deep blue aerosol products, *Reviews of Geophysics*, *50*(3).

Gkikas, A., E. Proestakis, V. Amiridis, S. Kazadzis, E. Di Tomaso, A. Tsekeri, E. Marinou, N. Hatzianastassiou, and C. Pérez García-Pando (2021), Modis dust aerosol (midas): a global fine-resolution dust optical depth data set, *Atmospheric Measurement Techniques*, *14*(1), 309–334.

Hedges, J., J. Baldock, Y. Gélinas, C. Lee, M. Peterson, and S. Wakeham (2002), The biochemical and elemental compositions of marine plankton: A nmr perspective, *Marine Chemistry*, *78*(1), 47–63.

Hersbach, H., B. Bell, P. Berrisford, S. Hirahara, A. Horányi, J. Muñoz-Sabater, J. Nicolas, C. Peubey, R. Radu, D. Schepers, et al. (2020), The era5 global reanalysis, *Quarterly Journal of the Royal Meteorological Society*, *146*(730), 1999–2049.

Hoffmann, D. L., M. Rogerson, C. Spötl, M. Luetscher, D. Vance, A. H. Osborne, N. M. Fello, and G. E. Moseley (2016), Timing and causes of north african wet phases during the last glacial period and implications for modern human migration, *Scientific Reports*, *6*(1), 1–7.

Holben, B. N., T. F. Eck, I. a. Slutsker, D. Tanre, J. Buis, A. Setzer, E. Vermote, J. A. Reagan, Y. Kaufman, T. Nakajima, et al. (1998), Aeronet—a federated instrument network and data archive for aerosol characterization, *Remote sensing of environment*, *66*(1), 1–16.

Jolly, D., I. C. Prentice, R. Bonnefille, A. Ballouche, M. Bengo, P. Brenac, G. Buchet, D. Burney, J.-P. Cazet, R. Cheddadi, et al. (1998), Biome reconstruction from pollen and plant macrofossil data for africa and the arabian peninsula at 0 and 6000 years, *Journal of Biogeography*, *25*(6), 1007–1027.

Kim, D., M. Chin, L. A. Remer, T. Diehl, H. Bian, H. Yu, M. E. Brown, and W. R. Stockwell (2017), Role of surface wind and vegetation cover in multi-decadal variations of dust emission in the sahara and sahel, *Atmospheric Environment*, *148*, 282–296.

Koren, I., Y. J. Kaufman, R. Washington, M. C. Todd, Y. Rudich, J. V. Martins, and D. Rosenfeld (2006), The bodélé depression: a single spot in the sahara that provides most of the mineral dust to the amazon forest, *Environmental Research Letters*, *1*(1), 014,005.

Korte, L. F., G.-J. A. Brummer, M. Van Der Does, C. V. Guerreiro, R. Hennekam, J. A. Van Hateren, D. Jong, C. I. Munday, S. Schouten, and J.-B. W. Stuut (2017), Downward particle fluxes of biogenic matter and saharan dust across the equatorial north atlantic, *Atmospheric Chemistry and Physics*, *17*(9), 6023–6040.

Kropelin, S., D. Verschuren, A.-M. Lézine, H. Eggermont, C. Cocquyt, P. Francus, J.-P. Cazet, M. Fagot, B. Rumes, J. M. Russell, et al. (2008), Climate-driven ecosystem succession in the sahara: the past 6000 years, *science*, *320*(5877), 765–768.

Kuper, R., and S. Kropelin (2006), Climate-controlled holocene occupation in the sahara: motor of africa's evolution, *science*, *313*(5788), 803–807.

Larrasoaña, J. C., A. P. Roberts, and E. J. Rohling (2013), Dynamics of green sahara periods and their role in hominin evolution, *PloS one*, *8*(10), e76,514.

Matthewson, A., G. Shimmield, D. Kroon, and A. Fallick (1995), A 300 kyr high-resolution aridity record of the north african continent, *Paleoceanography*, *10*(3), 677–692.

Myneni, R. B., F. G. Hall, P. J. Sellers, and A. L. Marshak (1995), The interpretation of spectral vegetation indexes, *IEEE Transactions on Geoscience and Remote Sensing*, *33*(2), 481–486.

Parker, A. O., M. W. Schmidt, Z. R. Jobe, and N. C. Slowey (2016), A new perspective on west african hydroclimate during the last deglaciation, *Earth and Planetary Science Letters*, *449*, 79–88.

Pinker, R. T., G. Idemudia, and T. Aro (1994), Characteristic aerosol optical depths during the harmattan season on sub-sahara africa, *Geophysical research letters*, *21*(8), 685–688.

Potts, R. (1998), Environmental hypotheses of hominin evolution, *American Journal of Physical Anthropology: The Official Publication of the American Association of Physical Anthropologists*, *107*(S27), 93–136.

Prospero, J. M., and T. N. Carlson (1972), Vertical and areal distribution of saharan dust over the western equatorial north atlantic ocean, *Journal of Geophysical Research*, *77*(27), 5255–5265.

Ridley, D., C. Heald, and J. Prospero (2014), What controls the recent changes in african mineral dust aerosol across the atlantic?, *Atmospheric Chemistry and Physics*, *14*(11), 5735–5747.

Rolph, G., A. Stein, and B. Stunder (2017), Real-time environmental applications and display system: Ready, *Environmental Modelling & Software*, *95*, 210–228.

Romero, O. E., G. Fischer, J. Karstensen, and P. Cermeño (2016), Eddies as trigger for diatom productivity in the open-ocean northeast atlantic, *Progress in Oceanography*, *147*, 38–48.

Schaebitz, F., A. Asrat, H. F. Lamb, A. S. Cohen, V. Foerster, W. Duesing, S. Kaboth-Bahr, S. Opitz, F. A. Viehberg, R. Vogelsang, et al. (2021), Hydroclimate changes in eastern africa over the past 200,000 years may have influenced early human dispersal, *Communications Earth & Environment*, *2*(1), 1–10.

Schepanski, K., I. Tegen, and A. Macke (2009), Saharan dust transport and deposition towards the tropical northern atlantic, *Atmospheric Chemistry and Physics*, *9*(4), 1173–1189.

Schepanski, K., B. Heinold, and I. Tegen (2017), Harmattan, saharan heat low, and west african monsoon circulation: modulations on the saharan dust outflow towards the north atlantic, *Atmospheric Chemistry and Physics*, *17*(17), 10,223–10,243.

Senut, B., M. Pickford, D. Gommery, and L. Ségalen (2018), Palaeoenvironments and the origin of hominid bipedalism, *Historical Biology*, *30*(1-2), 284–296.

Skonieczny, C., A. Bory, V. Bout-Roumazeilles, W. Abouchami, S. Galer, X. Crosta, A. Diallo, and T. Ndiaye (2013), A three-year time series of mineral dust deposits on the west african margin: sedimentological and geochemical signatures and implications for interpretation of marine paleo-dust records, *Earth and Planetary Science Letters*, *364*, 145–156.

Stanley, S. M. (1992), An ecological theory for the origin of homo, *Paleobiology*, *18*(3), 237–257.

Stein, A., R. R. Draxler, G. D. Rolph, B. J. Stunder, M. Cohen, and F. Ngan (2015), Noaa's hysplit atmospheric transport and dispersion modeling system, *Bulletin of the American Meteorological Society*, *96*(12), 2059–2077.

Taylor, C. M., P. P. Harris, and D. J. Parker (2010), Impact of soil moisture on the development of a sahelian mesoscale convective system: A case-study from the amma special observing period, *Quarterly Journal of the Royal Meteorological Society*, *136*(S1), 456–470.

Taylor, C. M., A. Gounou, F. Guichard, P. P. Harris, R. J. Ellis, F. Couvreux, and M. De Kauwe (2011), Frequency of sahelian storm initiation enhanced over mesoscale soil-moisture patterns, *Nature Geoscience*, *4*(7), 430–433.

Tierney, J. E., and P. B. deMenocal (2013), Abrupt shifts in horn of africa hydroclimate since the last glacial maximum, *Science*, *342*(6160), 843–846.

Tierney, J. E., P. B. deMenocal, and P. D. Zander (2017), A climatic context for the out-of-africa migration, *Geology*, *45*(11), 1023–1026.

van der Does, M., L. F. Korte, C. I. Munday, G.-J. A. Brummer, and J.-B. W. Stuut (2016), Particle size traces modern saharan dust transport and deposition across the equatorial north atlantic, *Atmospheric Chemistry and Physics*, *16*(21), 13,697–13,710.

van der Does, M., G.-J. A. Brummer, F. C. van Crimpen, L. F. Korte, N. M. Mahowald, U. Merkel, H. Yu, P. Zuidema, and J.-B. W. Stuut (2020), Tropical rains controlling deposition of saharan dust across the north atlantic ocean, *Geophysical Research Letters*, *47*(5), e2019GL086,867.

Voss, K. K., and A. T. Evan (2020), A new satellite-based global climatology of dust aerosol optical depth, *Journal of Applied Meteorology and Climatology*, *59*(1), 83–102.

Watrin, J., A.-M. Lézine, and C. Hély (2009), Plant migration and plant communities at the time of the "green sahara", *Comptes Rendus Geoscience*, *341*(8-9), 656–670.

Weldeab, S., R. R. Schneider, M. Kolling, and G. Wefer (2005), Holocene african droughts relate to eastern equatorial atlantic cooling, *Geology*, *33*(12), 981–984.

Wood, B. (1996), Human evolution, *Bioessays*, *18*(12), 945–954.

Yu, H., Q. Tan, M. Chin, L. A. Remer, R. A. Kahn, H. Bian, D. Kim, Z. Zhang, T. Yuan, A. H. Omar, et al. (2019), Estimates of african dust deposition along the trans-atlantic transit using the decadelong record of aerosol measurements from caliop, modis, misr, and iasi, *Journal of Geophysical Research: Atmospheres*, *124*(14), 7975–7996.

Zielhofer, C., H. von Suchodoletz, W. J. Fletcher, B. Schneider, E. Dietze, M. Schlegel, K. Schepanski, B. Weninger, S. Mischke, and A. Mikdad (2017), Millennial-scale fluctuations in saharan dust supply across the decline of the african humid period, *Quaternary Science Reviews*, *171*, 119–135.